A brief introduction to oceanic waves

April 16, 2015

Daniel Whitt
Department of Applied Mathematics and Theoretical Physics
University of Cambridge
dw494@cam.ac.uk
http://www.damtp.cam.ac.uk/user/dw494

1 Introduction: A tale of three waves

The first of two lectures to be delivered at Capital Normal University, Beijing
March 30-April 3, 2015

Many textbooks treat oceanic wave motion extensively (e.g. Phillips, 1966; Leblond and Mysak, 1978; Lighthill, 1978; Gill, 1982; Pedlosky, 1986; 2003) and the ideas have been studied for many centuries (e.g. the tidal equations were first derived by Pierre-Simon Laplace in 1776). As a result, I can't possibly give either a particularly original or comprehensive treatment of oceanic wave motions in this first lecture. Previous researchers and teachers deserve much (if not all) of the credit for what appears here.

Rather, my goal is to give a descriptive introduction to oceanic wave motions using both observations and mathematical analysis. My hope is that after this lecture you will have some appreciation for 1) the ubiquity and diversity of wave phenomena in the ocean, and 2) the principle mathematical models and techniques that have been used to interpret and understand these motions in atmospheric science, oceanography and geophysical fluid dynamics.

In the second lecture, I will build on these ideas by discussing some topics in ocean wave physics that are "special" in that I have worked on them and/or the topic particularly interests me.

1.1 Introduction

The ocean can support a variety of classes of waves (*which we loosely define as traveling perturbations to an equilibrium background state with a propagation speed that is typically different from the background flow speed*). These classes are distinguished by the dominant restoring forces to a given departure from the equilibrium, including e.g. frictional, gravitational, pressure, and inertial forces (we entirely ignore negligible electromagnetic forces in the dynamics of Earth's ocean). Strictly speaking, all of the possible forces tend to be acting to some degree at all spatio-temporal scales. However, there is often a great deal to be learned about the dynamics of the ocean by isolating

the mechanics associated with the dominant restoring force (or forces) at a particular scale (time and space or, equivalently, frequency and wavelength) and investigating the physics of a reduced physical and mathematical model.

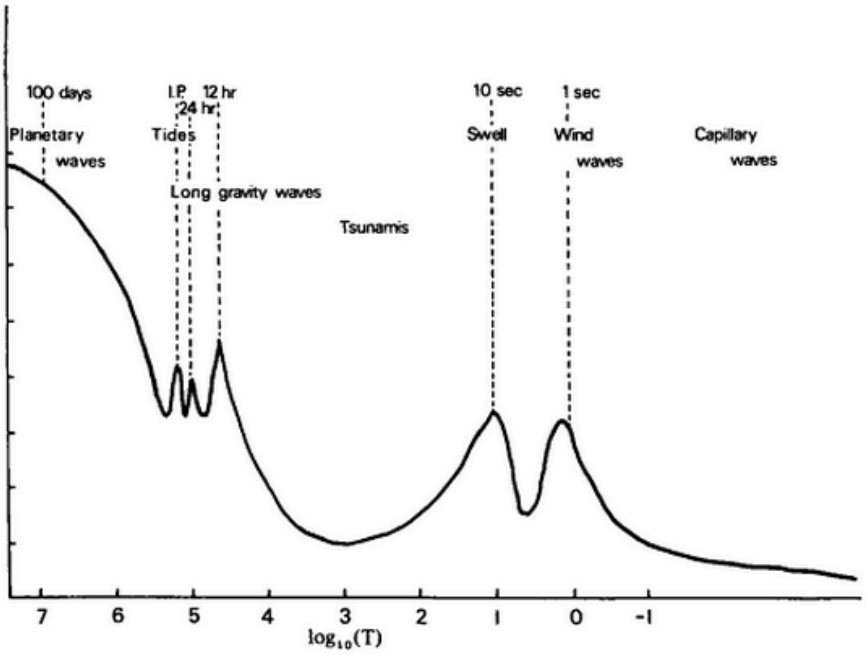

Figure 1: Schematic of the energy spectrum of ocean variability. From Leblond and Mysak (1978) *Waves in the ocean.*

This is because the governing physical model (the Navier-Stokes system) describes an extreme diversity of phenomena; characteristic length scales range from thousands of km (such as those associated with planetary waves and synoptic weather patterns in the atmosphere) to mm (such as capillary waves in a lake) and time scales range from seconds to months (see Figure 1).[1] Both the time and space scales of typical wave motions range over more than 7 orders of magnitude in the ocean (see e.g. Figure 1). Even if analytic solutions to the Navier Stokes equations were always available, a detailed investigation of the properties of the different solutions would still be necessary to understand the practical implications of the different solutions (of course analytic solutions are also extremely hard to obtain and existence and uniqueness proofs are arguably among the most important unsolved problems in all mathematics).

1.2 Equations of Motion

As I already suggested, the governing mathematical model for all the wave phenomena to be discussed is the rotating, incompressible, Navier-Stokes system. In the context of Earth, these equations are best presented in spherical coordinates. However, here we will consider motions that can be studied using local tangent-plane geometries where Cartesian coordinates are appropriate

[1] At the outset, we neglect sound waves, which require a compressible set of equations and have a negligible impact on the dynamics.

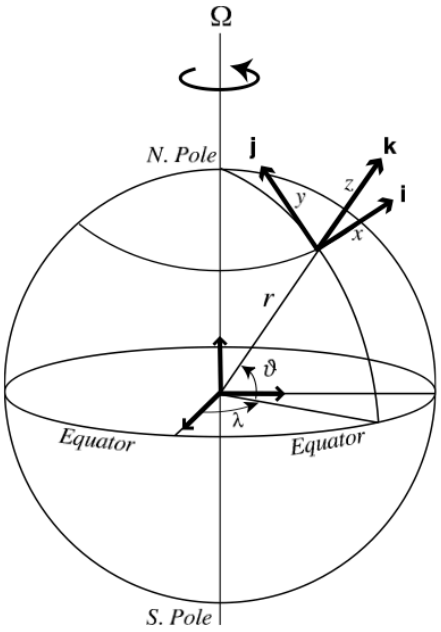

Fig. 2.3 The spherical coordinate system. The orthogonal unit vectors **i**, **j** and **k** point in the direction of increasing longitude λ, latitude ϑ, and altitude z. Locally, one may apply a Cartesian system with variables x, y and z measuring distances along **i**, **j** and **k**.

Figure 2: A schematic of our coordinate system, from *Vallis's* Atmospheric and Oceanic Fluid Dyn. textbook.

(see Figure 2). Moreover, because the density varies by no more than about 1% from the background value of $\rho_0 \approx 1025$ kg/m^3, we include the local density (as opposed to the reference density) only when multiplied by gravity. This simplification is known as the *Boussinesq approximation*. These equations of motion can be written:

$$\underbrace{\frac{\partial \mathbf{u}}{\partial t}}_{\text{Time tendency}} + \underbrace{\mathbf{u}\cdot\nabla\mathbf{u}}_{\text{Advection}} + \underbrace{\mathbf{f}\times\mathbf{u}}_{\text{Coriolis}} = -\underbrace{\frac{\nabla p}{\rho_0}}_{\text{Pressure Gradient}} + \underbrace{\mathbf{b}}_{\text{Buoyancy}} + \underbrace{\nu\Delta\mathbf{u}}_{\text{Friction}}, \tag{1}$$

$$\frac{\partial b}{\partial t} + \mathbf{u}\cdot\nabla b = \kappa\Delta b, \tag{2}$$

$$\nabla\cdot\mathbf{u} = 0, \tag{3}$$

The ∇ is the three-dimensional gradient operator, $\Delta = \nabla\cdot\nabla$ is the three-dimensional Laplacian operator, $\times$ denotes the vector cross-product and $\nabla\cdot$ denotes the three-dimensional divergence operator. The three-dimensional velocity vector field $\mathbf{u} = (u, v, w)$ (in units of m/s) points locally to the east, north and upwards respectively in the direction of unit vectors $(\mathbf{i}, \mathbf{j}, \mathbf{k})$ (see Figure 2). The buoyancy force $\mathbf{b} = (0, 0, b)$ defines the local vertical, where $b = -g\rho/\rho_0$. In the ocean, the density ρ (in units of kg/m^3) depends non-linearly on two tracers (temperature and salinity), which diffuse at different rates. Moreover, the density also depends weakly on pressure. In this presentation, I will ignore these subtleties and assume that the density can be modeled as a single tracer with a single molecular diffusivity κ (in units of m^2/s with the same magnitude as the kinematic viscosity ν),

e.g. as if the density depends linearly on temperature. The gravity g includes the true gravitational acceleration modified by a small centrifugal acceleration (the modification to $g = 9.81$ m/s^2 due to the centrifugal force is of the order of 0.3% so it is safe to ignore it here). The Coriolis force reduces to $\mathbf{f} \times \mathbf{u} = (-fv, fu, 0)$ because we keep only the local vertical component of the Coriolis vector so that $\mathbf{f} = (0, 0, 2\Omega_e \sin(\theta))$ where $\Omega_e \approx 7.3 \times 10^{-5}$ s^{-1} is the angular rotation rate of Earth and θ is the local latitude (see Figure 2). When I consider large scale Rossby wave motions, I will define a *beta plane* where $f = f_0 + \beta y$ is a linear function of the y coordinate. Otherwise, $f = f_0 \approx 10^{-4}$ s^{-1} in the mid-latitudes.[2]

Now we will derive governing equations and wave solutions for three different classes of wave motion, with characteristic horizontal scales ranging from small ($\sim 1 - 100$ m) to large (~ 100 km) and timescales ranging from short (a few seconds) to long (at least a few days). The three classes are: 1) waves at the air/water interface, 2) internal inertia-gravity waves in a rotating, density-stratified fluid, 3) Rossby waves in a stratified fluid with a variable rotation rate (i.e. on a beta-plane).

1.3 Example 1: Surface gravity waves

Probably the most familiar class of ocean wave is the surface gravity wave at the air-water interface. These motions are characterized by periods of a few seconds, much shorter than the rotational period of Earth (see Figure 1). They can be generated locally by winds applied over a short "fetch" or they may propagate in from afar as "swell" generated by a large storm. Figure 3 shows an image of surface waves shoaling at a beach.

Figure 3: A photograph of surface gravity waves shoaling as they approach a beach. From http://www.blog.buoyalarm.com/how-to-read-ocean-buoys-tips-resources.

Here I will introduce a simple model for wave propagation (that does not describe the generation or dissipation process) based on several simplifications of the governing equations (1). Suppose the wave motion has a characteristic time scale $\tilde{T} = 2\pi/\tilde{\omega}$, length scale $\tilde{L} = 2\pi/\tilde{k}$ (both horizontal and vertical), and velocity scale $\tilde{U}$, where $\tilde{\omega}$ is the characteristic scale for the wave frequency and $\tilde{k}$ is the characteristic scale for the horizontal wave number (in general, tildes will denote characteristic

[2]See e.g. Vallis, (2006) *Atmospheric and Oceanic Fluid Dynamics* or Phillips (1966), *The dynamics of the upper ocean* or any of a number of similar textbooks for more on the equations of motion.

scales rather than the dynamical variables). Note the crucial implicit assumption that the aspect ratio of the motion is order one, that is the vertical length scale and velocity scale is equivalent to the horizontal length and velocity scale,

$$\tilde{U} \sim \tilde{V} \sim \tilde{W}, \tag{4}$$

$$\tilde{L} \sim \tilde{H}, \tag{5}$$

and that the pressure scales with the acceleration term $\tilde{P} \sim \tilde{U}\tilde{\omega}/\tilde{k}$. Then we apply the following *explicit* assumptions:

1. The wave frequency is much larger than the Coriolis frequency so that the time tendency is much greater than the Coriolis force in (1). That is,

$$\frac{f}{\tilde{\omega}} << 1. \tag{6}$$

2. The wave has a sufficiently small characteristic velocity U that the advective terms are much smaller than the time tendency in (1). That is,

$$\frac{\tilde{U}\tilde{k}}{\tilde{\omega}} << 1. \tag{7}$$

3. The wave motion is not affected by friction; the time tendency is much larger than the dissipative term. That is,

$$\frac{\nu\tilde{k}^2}{\tilde{\omega}} << 1. \tag{8}$$

In any all three cases the significance of the respective forces has been expressed as a ratio of two time scales or, equivalently, a ratio of two frequencies.

As an aside, note that the assumption of an order-one aspect ratio and a characteristic timescale that is much shorter than the advective timescale implies that density perturbations have a negligible effect on gravity wave motion and the fluid can be treated as if it has a uniform density. Incidentally, this implies that the motion has a frequency that is much larger than the local *buoyancy frequency*,

$$\omega >> N = \sqrt{\frac{\partial b}{\partial z}} = \sqrt{\frac{-g}{\rho_0}\frac{\partial \rho}{\partial z}}. \tag{9}$$

In general, one should consider carefully the limitations of the different assumptions. Often the analysis of where and how the assumptions break down is more illuminating than the results of the analysis assuming the assumptions are hold. Moreover, it is even more important to consider the consequences of the implicit scaling assumptions. Were the implicit assumptions about length and time scales really justified in this case? What happens if the aspect ratio of the wave motion changes?

In any case, the resulting equations for short, high frequency gravity waves are

$$\underbrace{\frac{\partial \mathbf{u}}{\partial t}}_{\text{Time tendency}} = - \underbrace{\frac{\nabla p}{\rho_0}}_{\text{Pressure Gradient}} + \underbrace{\mathbf{g}}_{\text{Buoyancy}}, \tag{10}$$

$$\nabla \cdot \mathbf{u} = 0, \tag{11}$$

The illuminating result comes from taking the curl of these equations, which yields

$$\frac{\partial \nabla \times \mathbf{u}}{\partial t} = 0, \tag{12}$$

which is to say the flow in short linear surface gravity waves is *irrotational*. The vorticity $\nabla \times \mathbf{u}$ does not evolve with time (and hence the explicitly time dependent wave motion has no vorticity).

By the *Helmholtz Theorem* (also known as the fundamental theorem of vector calculus), we can decompose any arbitrary vector field in a compact three-dimensional domain into a divergent and rotational part, that is:

$$\mathbf{u} = \underbrace{\nabla \phi}_{\text{irrotational/divergent}} + \underbrace{\nabla \times \mathbf{\Phi}}_{\text{solenoidal/rotational}}, \tag{13}$$

where $\nabla \cdot \mathbf{\Phi} = 0$.[3] In the case of the water wave equations, the rotational part is 0 (we are only interested in the oscillatory part of the solution, which has no curl), and the flow is entirely described by the Laplace equation:

$$0 = \nabla \cdot \mathbf{u} = \Delta \phi. \tag{15}$$

Of course, the dynamics emerge from the boundary conditions. The bottom boundary condition is straightforward,

$$\frac{\partial \phi}{\partial z} = 0, \text{ at } \; z = -D. \tag{16}$$

At the surface, there are two conditions:

1. The *kinematic* condition states that the vertical velocity at the surface is equal to the change in surface height,
$$w|_{z=\zeta} = \frac{\partial \phi}{\partial z}|_{z=\zeta} = \frac{\partial \zeta}{\partial t} + \nabla_h \phi \cdot \nabla_h \zeta, \tag{17}$$
where $\nabla_h = (\partial/\partial x, \partial/\partial y)$.

2. The *dynamic* condition states that the pressure difference across the free surface is equal to zero.

The governing equations can be written as

$$\frac{\partial \nabla \phi}{\partial t} = -\frac{\nabla p}{\rho} - g \nabla z, \tag{18}$$

[3]With regards to the uniqueness/non-uniqueness of the Helmholtz decomposition, consider an alternative ϕ' and $\mathbf{\Phi}'$ such that,

$$0 = \nabla(\phi - \phi') + \nabla \times (\mathbf{\Phi} - \mathbf{\Phi}'). \tag{14}$$

If we take the divergence, we find that $\Delta f = 0$ where $f = \phi - \phi'$ is a solution. In order to satisfy the original Helmholtz decomposition, $\nabla \times (\mathbf{\Phi} - \mathbf{\Phi}') = -\nabla f$, which we can define for any f. So in the absence of boundary conditions, the scalar potential is only unique up to a harmonic function. In a domain without boundary (e.g. the surface of a sphere), there are no non-trivial harmonic functions f because of the maximum principle (harmonic functions can have no local interior maxima, see e.g. Evans' *Partial Differential Equations*). However, on a compact domain (e.g. an annulus or a square), boundary conditions on ϕ are required to eliminate the possibility of a non-trivial harmonic function f. Alternatively, as discussed by Chorin and Marsden, the rotational part of the decomposition must be parallel to the boundary, that is $(\nabla \times \mathbf{\Phi}) \cdot \mathbf{n} = 0$ on the boundary, where $\mathbf{n}$ is the boundary normal vector. See e.g. Wu, Ma and Shu (2006), *Vorticity and Vortex Dynamics* or Chorin and Marsden (1993), *A Mathematical Introduction to Fluid Mechanics*.

which implies

$$\nabla\left(\frac{\partial\phi}{\partial t}+\frac{p}{\rho}+gz\right)=0. \tag{19}$$

and

$$\frac{\partial\phi}{\partial t}+\frac{p}{\rho}+gz=0, \tag{20}$$

where we can add an arbitrary function of time to ϕ to make it satisfy this equation. At $z=\zeta$,

$$\frac{\partial\phi}{\partial t}+\frac{p_a}{\rho_0}+g\zeta=0, \tag{21}$$

where p_a is the atmospheric pressure, which we will set equal to zero. We will neglect surface tension altogether, although this effect is important for wave generation. To be consistent with the reduced linearized equations we have chosen, this boundary condition should actually be applied at $z=0$ for small ζ (one can infer this by constructing a Taylor series expansion for the terms in the boundary condition about $\zeta=0$ and noting that only the zeroth order terms of order ζ, consistent with our linearization). Thus, at $z=0$,

$$\frac{\partial^2\phi}{\partial t^2}+g\frac{\partial\phi}{\partial z}=0. \tag{22}$$

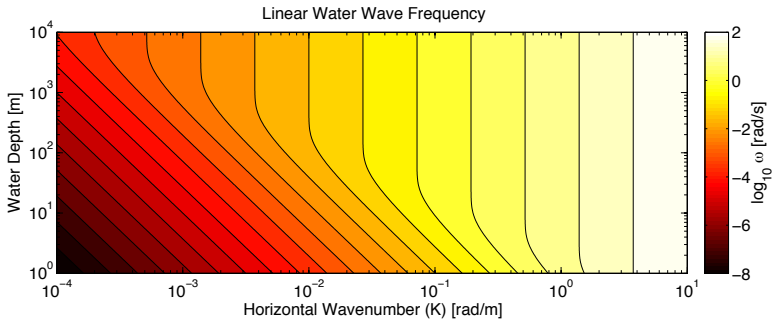

Figure 4: A plot of the dispersion relation for linear water waves as a function of the magnitude of the horizontal wavenumber K and the water depth D.

We look for plane wave solutions of Laplace's equation that satisfy the top and bottom boundary conditions and are periodic in x, y and t,

$$\phi=Re(R(z)e^{i(kx+ly-\omega t)}) \tag{23}$$

We solve the resulting ordinary differential equation for the vertical structure

$$\frac{d^2R}{dz^2}=K^2R, \tag{24}$$

where $K^2=k^2+l^2$. The general solution of (24) is of the form $R=Ae^{Kz}+Be^{-Kz}$ and the bottom boundary condition restricts the solution to be of the form: $R=A'\cosh(K(z+D))$. Enforcing the condition at $z=0$ implies

$$-\omega^2\cosh(KD)+gK\sinh(KD)=0 \tag{25}$$

which can be rewritten as

$$\omega = \pm\sqrt{gK\tanh(KD)}. \tag{26}$$

This is the *dispersion relation*, plotted as a function of K and D in Figure 4. It describes how the frequency of water waves varies with wavenumber and water depth. It is a key result of this theory that the frequency and *phase speed* (ω/K) depend on wavenumber and depth. This means that in contrast to the solutions of the classic wave equation, which travel without changing shape, the different Fourier components of these solutions will become separated in space as they propagate.

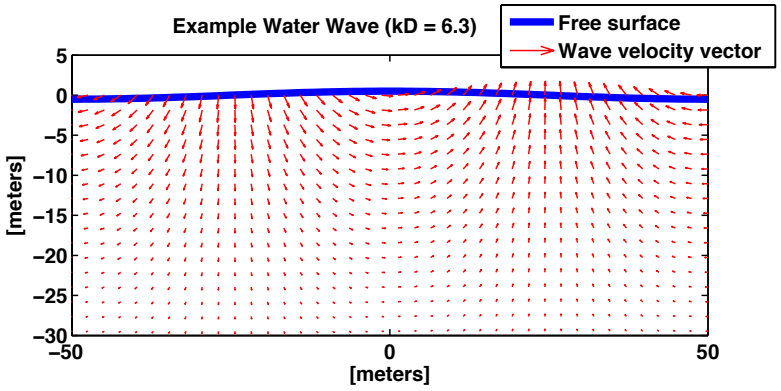

Figure 5: An example gravity wave solution for a wave with 100 m wavelength in 100 m of water. The free surface displacement amplitude is 0.5 m.

What do these solutions look like, (assuming $K = k$ and $l = 0$, i.e. the wave propagates in the x direction)? We can use the solutions derived above to obtain the following formulas:

$$\zeta(x,t) = \zeta_0 \cos(kx - \omega t), \tag{27}$$

$$\phi(x,z,t) = \zeta_0 \frac{\omega}{k} \frac{\cosh k(z+D)}{\sinh KD} \sin(kx - \omega t), \tag{28}$$

$$u = \zeta_0 \omega \cos(kx - \omega t) \frac{\cosh k(z+D)}{\sinh KD}, \tag{29}$$

$$w = \zeta_0 \omega \sin(kx - \omega t) \frac{\sinh k(z+D)}{\sinh KD}. \tag{30}$$

There are two regimes, separated by the magnitude of KD. If $KD << 1$ the solutions are for shallow water waves, whereas if $KD >> 1$ the solutions are for deep water waves. However, we must be careful because in some parts of the parameter space shown in Figure 4 the assumptions used to derive the governing equations do not hold. An obvious example is the neglect of rotational effects, which become important at mid-latitudes for $\omega \lesssim 10^{-4}$ s^{-1}. In any case, an example wave velocity field for intermediate KD is shown in Figure 5.

One can follow this analysis with an investigation of how these waves propagate (both wave phase and wave energy), one could consider an initial value problem given an arbitrary disturbance, and one could consider solutions with multiple frequencies present, among other perspectives. We will not pursue these avenues with this class of waves—but see Pedlosky (2003) *Waves in the ocean and atmosphere* and Phillips (1966) *Upper Ocean Dynamics* for a more in depth discussion.

1.4 Example 2: Internal inertia-gravity waves

Instead we will turn to another class of wave motion, *internal waves*. In most places, the ocean is strongly stratified in density and the dominant force balance is *hydrostatic*, that is the vertical pressure gradient is in balance with the buoyancy force

$$0 = -\frac{1}{\rho_0}\frac{\partial \overline{p}(z)}{\partial z} - g\frac{\overline{\rho}(z)}{\rho_0} = -\frac{1}{\rho_0}\frac{\partial \overline{p}(z)}{\partial z} + \overline{b}(z), \tag{31}$$

and all interior wave motions are a small perturbation to this. For example, a typical background density profile in the North Atlantic is shown in Figure 6.

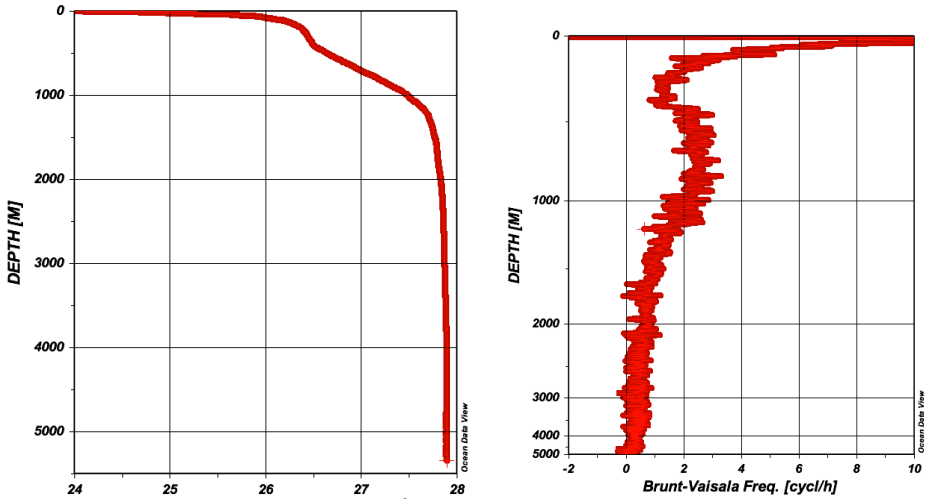

Figure 6: (Left)Density anomaly (from 1000 kg/m^3) as a function of depth in the ocean. The density is adiabatically normalized to an equivalent density at the ocean surface. This is known as the *potential density*. It effectively removes the dependence on pressure from the equation of state. (Right) Buoyancy frequency N, also known as the Brunt Vaisala frequency. Note the stretched depth axis.

To derive the internal wave governing equations, I subtract the background hydrostatic balance (31) from (1) to obtain the governing equations for the wave perturbation (I do not relabel p and b—the fact that these variables are perturbations from a background hydrostatic balance is implied).

$$\frac{\partial u}{\partial t} - f_0 v = -\frac{1}{\rho_0}\frac{\partial p}{\partial x}, \tag{32}$$

$$\frac{\partial v}{\partial t} + f_0 u = -\frac{1}{\rho_0}\frac{\partial p}{\partial y}, \tag{33}$$

$$\frac{\partial w}{\partial t} = -\frac{1}{\rho_0}\frac{\partial p}{\partial z} + b, \tag{34}$$

$$\frac{\partial b}{\partial t} + wN^2(z) = 0, \tag{35}$$

$$\frac{\partial u}{\partial x} + \frac{\partial v}{\partial y} + \frac{\partial u}{\partial z} = 0, \tag{36}$$

where $N^2 = \partial\bar{b}/\partial z$. The equations are the same as the gravity wave equations with the following exception: I have relaxed the assumption that $\omega >> N >> f$ (but we assume that the horizontal scale is small enough that $f = f_0$ is constant). Hence, the Coriolis terms may be important and, moreover, buoyancy variations may be significant. Note that, as in the previous discussion, we have assumed that the perturbation amplitudes are small enough that non-linear terms (which scale as wave amplitude squared) are small enough that we can neglect them, i.e. $Uk/\omega << 1$, and that friction is sufficiently weak that we may neglect those terms as well, i.e. $\nu\omega/L^2 << 1$.

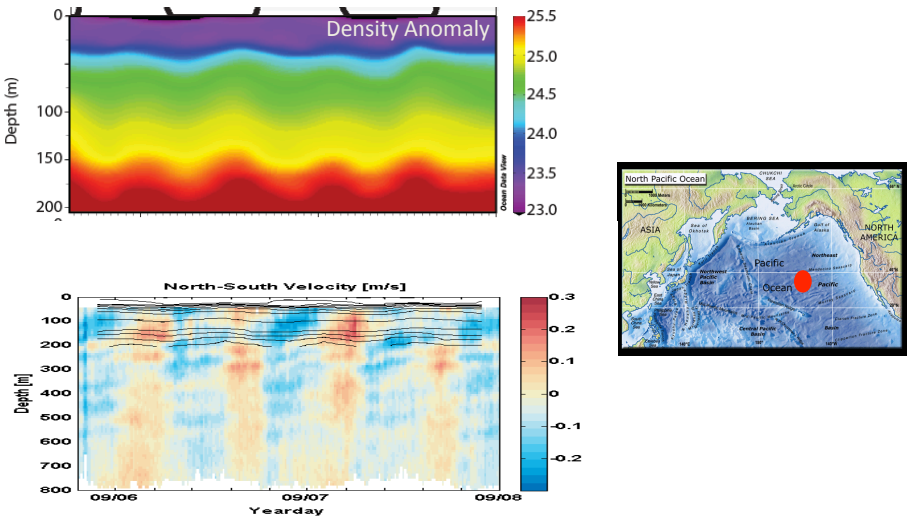

Figure 7: (Top Left) Density anomaly (kg/m^3) observed over two days (September 6 - September 8, 2014) of repeated profiles in the north Pacific subtropical gyre (Bottom Left) time series of north/south velocity, and (Right) a map showing location of the observations.

Although perhaps unfamiliar to the casual observer, examples of internal wave motion are quite common in oceanic observations. See, for example, the observed semi-diurnal oscillatory velocity and density patterns in Figure 7, presumably generated by tides oscillating over the Hawaiian ridge several 100 km to the south of the sampling location. Alternatively, consider Figure 8, which shows prominent circular near-inertial oscillations with $\omega \approx f$ observed in the ocean boundary layer after the passage of a storm in the north Pacific. Because tides sloshing over rough topography and winds are the dominant sources of energy for internal waves (I will discuss why later), frequency spectra show marked peaks in energy near the dominant semi-diurnal tidal frequency and local inertial frequency (Figure 9). However, both vertical wavenumber and frequency spectra show that like surface gravity waves, internal waves are perhaps best represented by a continuum of frequencies and wave numbers that interact non-linearly. In fact, the observations of the internal wave continuum (excluding the peaks in frequency space) are so robust that some have argued that the internal wave spectrum takes on a universal shape (e.g. Chris Garrett and Walter Munk 1972, *Space-Time Scales of Internal Waves*). However, although there is some theoretical support for this model, it still must be viewed as an empirical fit to observations. Explaining why it is nearly universal (and why and how spectra deviate from this form in certain cases) remain important open questions in internal wave research (see e.g. Polzin and Lvov *Toward Regional Characterizations*

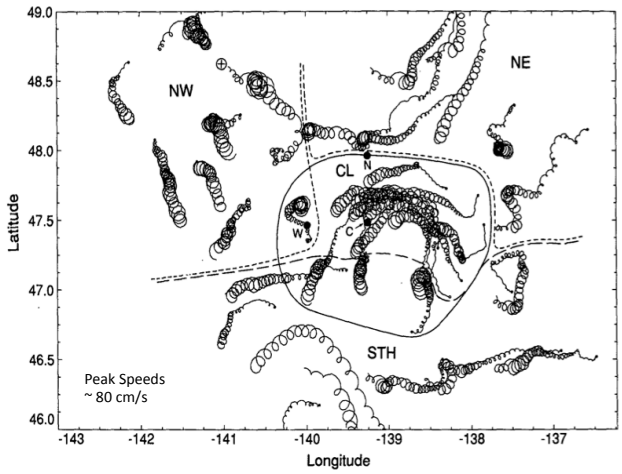

Figure 8: Twenty-five days of surface drifter trajectories after a storm in the eastern north Pacific. The drifters trajectories represent a combination of decaying inertial motions (circular oscillations) and weak geostrophic flow (the time-averaged drift). From D'Asaro et al. (1995), *Upper ocean inertial currents forced by a strong storm.*

of the Oceanic Internal Wavefield).

To investigate the basic properties of linear internal waves, we reduce the system of equations to one governing wave equation for the vertical velocity,

$$\left(\frac{\partial^2}{\partial t^2} + f_0^2\right)\frac{\partial^2 w}{\partial z^2} + \left(\frac{\partial^2}{\partial t^2} + N^2(z)\right)\left(\frac{\partial^2 w}{\partial x^2} + \frac{\partial^2 w}{\partial y^2}\right) = 0, \tag{37}$$

with $w = 0$ at the top and bottom boundaries (we assume the top surface is rigid, this eliminates the usually-small barotropic or depth-independent solution). In two dimensions, we can write (37) in terms of a stream function ψ, where $\partial\psi/\partial z = v$ and $\partial\psi/\partial y = -w$, that is

$$\left(\frac{\partial^2}{\partial t^2} + f_0^2\right)\frac{\partial^2 \psi}{\partial z^2} + \left(\frac{\partial^2}{\partial t^2} + N^2(z)\right)\frac{\partial^2 \psi}{\partial y^2} = 0. \tag{38}$$

The variation of N with depth suggests looking for plane wave solutions in the horizontal that have a vertical structure depending on the details of N. We thus proceed by looking for solutions of the form $\psi = \psi_0(z)e^{i(ly-\omega t)}$. Inserting this ansatz into (38) yields the following system:

$$\frac{d^2\psi_0}{dz^2} + m^2\psi_0 = 0, \tag{39}$$

where

$$m^2 = l^2\frac{(N^2(z) - \omega^2)}{(\omega^2 - f_0^2)}, \tag{40}$$

with a boundary condition of $\psi = 0$ at the top and bottom (a similar equation can be derived for the vertical displacement or vertical velocity). In the presence of constant stratification N, the solutions are $\psi_0(z) = \sin(mz)$, where $m = \pi j/D$ with $j = 1, 2, ...$ a natural number. In

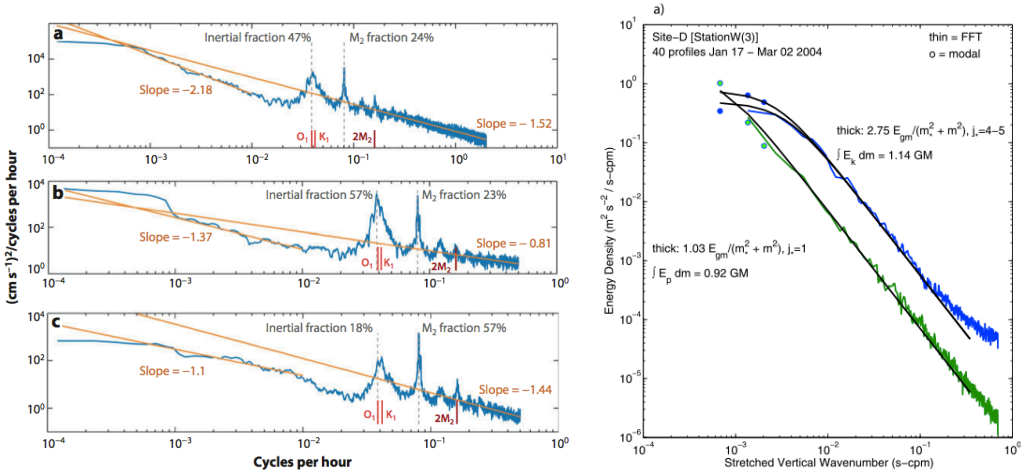

Figure 9: (Left) Frequency power spectra observed at various depths in the North Atlantic. Peaks are seen near the local inertial frequency f_0 and the semi-diurnal tidal frequency M_2, showing that there is elevated internal wave energy at these frequencies. From Ferrari and Wunsch (2009), *Ocean Circulation Kinetic Energy: Reservoirs, Sources and Sinks* (Right) Wavenumber power spectra from a site near Cape Cod, MA show that potential and kinetic energy scale as vertical wavenumber to the -2 power. This is a *nearly* universal property of oceanic kinetic and potential energy vertical wavenumber spectra. From Polzin and Lvov (2011), *Toward regional characterizations of the oceanic internal wave field*

general, one can solve for the vertical structure functions numerically—there is always a discrete set and they form a complete basis for any arbitrary vertical structure function satisfying the boundary conditions. However, variable stratification stretches the mode structure, concentrating the oscillations in regions where there is larger stratification (see Figure 10).[4]

The motions with large vertical wavelengths (i.e. the gravest modes or *low modes*) will clearly be influenced by the top and bottom of the ocean. Hence, the ducted solutions discussed above are appropriate. However, the wave motions with smaller vertical scales or high modes could potentially be isolated in three spatial dimensions (there is less but certainly non-negligible energy in higher modes, see Figure 9). As a result, it makes more sense to consider pure plane waves as a fundamental solution for these structures,

$$\psi = Re(\psi_0 e^{i(kx+ly+mz-\omega t)}). \tag{41}$$

Upon substitution of this equation into the governing system, we obtain the following dispersion relation,

$$\omega/f = \pm\sqrt{\frac{1+\frac{N^2}{f_0^2}\frac{k_H^2}{m^2}}{1+\frac{k_H^2}{m^2}}} \tag{42}$$

[4]Alternatively, one can perform a vertical coordinate stretching to remove this effect, as discussed in Eckart (1961), *Internal waves in the ocean.*

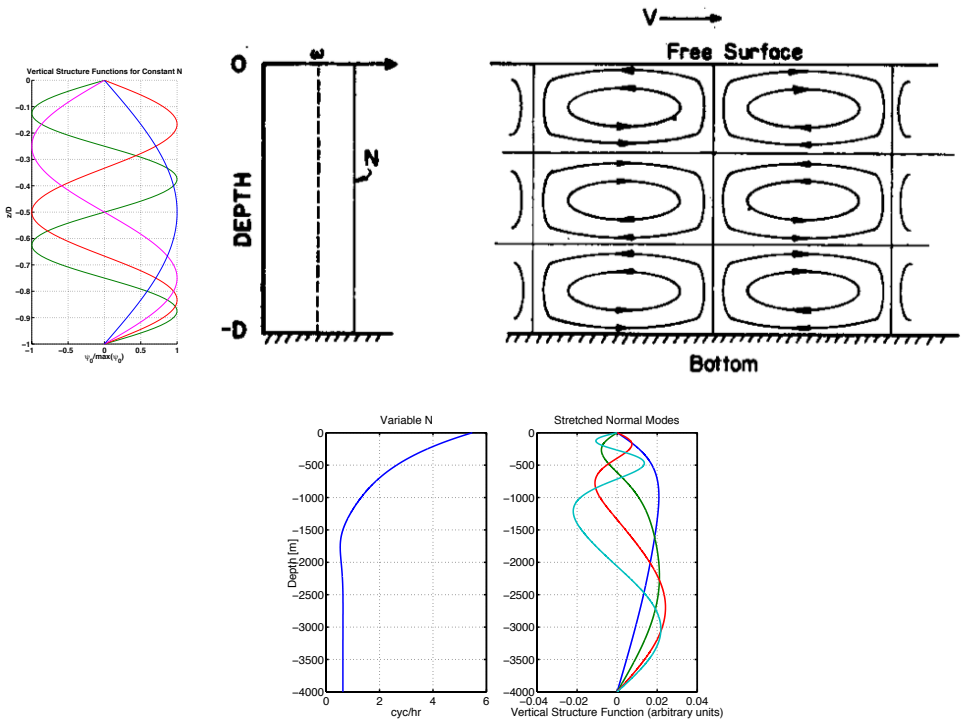

Figure 10: (Top Left) Structure functions for the 4 gravest vertical modes in constant stratification. (Top Right) An image of the spatial pattern in the horizontal vertical plane for the third gravest mode. (the latter image is from Eckart (1961), *Internal Waves in the Ocean*. (Bottom) Example stratification and vertical structure functions for the 4 gravest modes in an ocean with variable stratification.

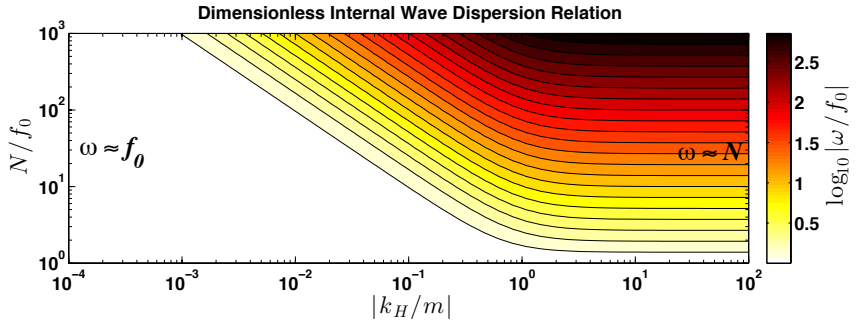

Figure 11: The dimensionless internal wave dispersion relation (42).

where $k_H = \sqrt{k^2 + l^2}$ and N is assumed to be locally constant but might vary slowly on the scale of a wavelength. The dispersion relation depends on two parameters N/f_0 (called the inverse of Prandtl's ratio) and $|k_H/m|$ (the wave aspect ratio)—see Figure 11. The ducted solution in an ocean with constant N must also satisfy (42) and Eckart (1961, *Internal waves in the ocean*)

showed that for waves with $f_0 < \omega < N$, one can simply stretch the vertical coordinate to reduce a variable N problem to an analogous one with constant N.

What is interesting about this dispersion relation is that in a constant medium, the angle with respect to the horizontal (aspect ratio) is fixed by the frequency. This is in stark contrast to many familiar waves that radiate in all directions from a source, regardless of frequency (e.g. sound, light etc.). Here, the waves radiate in a cone away from the source. Excellent laboratory visualizations of this phenomenon have been presented by Mowbray and Rarity (1967) *A theoretical and experimental investigation of the phase configuration of internal waves of small amplitude in a density stratified liquid* (see Figure 12). Others have explored some of the unusual reflection dynamics that result. See Figure 13 for two examples from laboratory experiments.

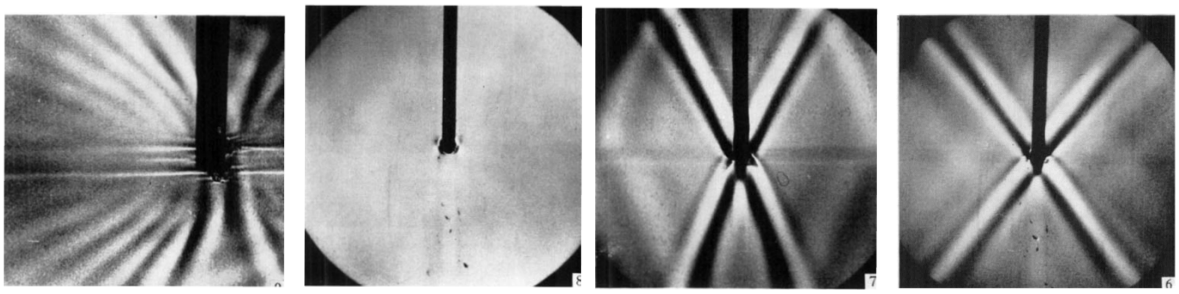

Figure 12: Laboratory visualizations of internal waves radiating from an oscillating rod in a stratified tank with nearly constant N. The first image is of waves produced by a transient disturbance. And then by oscillations with frequencies $\omega = 1.1N, 0.9N, 0.7N$. From Mowbray and Rarity (1967) *A theoretical and experimental investigation of the phase configuration of internal waves of small amplitude in a density stratified liquid.*

1.5 Example 3: Rossby waves

In the third example, I'd like to discuss oceanic Rossby waves (continuing on our trajectory from small to large length and time scales). These are wave motions at the opposite end of the spectrum from water waves (see Figure 1), with frequencies much smaller than the Earth's angular frequency, $\omega << f_0$. However, these waves are perhaps even more important for human society, although they may not appear as "wavelike" as the ocean surf (e.g. Petoukov et al. 2013, *Quasiresonant amplification of planetary waves and recent Northern Hemisphere weather extremes*; also look for several comments/follow-up articles that question the interpretation of Petoukov et al.). As schematically shown in Figure 1, motions with the spatio-temporal scales of Rossby waves have much more energy than the motions at smaller scales. They play a central role in any dynamical theory of the large scale circulation of the ocean and atmosphere. Moreover, any weather model must be able to make a very accurate description of Rossby wave activity (however, even doing this is not enough for a perfect forecast!). Although Rossby waves are not as obvious as surface gravity waves to the casual observer of the ocean, satellite altimeters (which measure sea surface height anomalies) have facilitated very precise measurements of Rossby wave activity in the oceanic domain. For example, Figure 14 shows low-pass filtered longitude time plots of ocean sea surface height in the Pacific. These images exhibit distinct oscillating banded patterns moving towards the west. These patterns

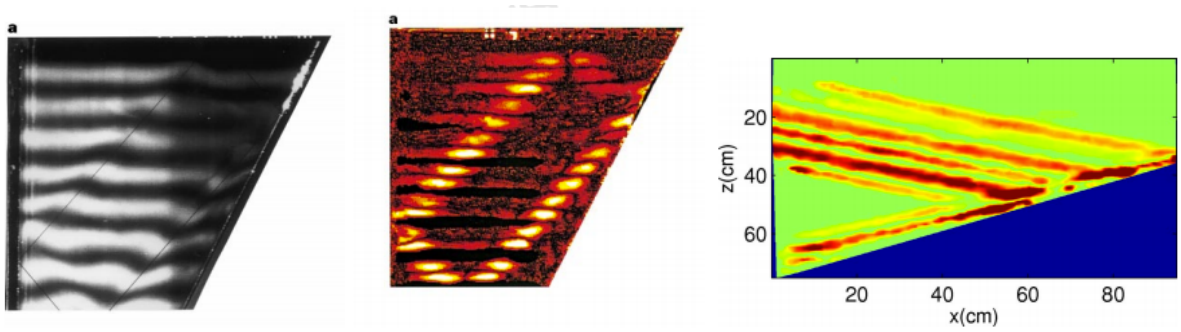

Figure 13: Laboratory visualizations internal wave motion with a nearly constant frequency in constant stratification. (Left two) The wave motions are trapped in an attractor because of the unusual dispersion relation. From Maas et al. (1997), *Observation of an internal wave attractor in a confined stably stratified fluid.* (right) observations of a constant frequency internal wave incident on a slope parallel to the wave aspect ratio (in a tank with constant N) results in critical reflection and large energy dissipation at the boundary. From Gostiaux et al. (2006), *Quantitative laboratory investigations of internal wave reflections on ascending slopes.*

are the signature of Rossby waves, the subject of our current investigation. Let's see if we can predict this westward phase propagation.

As in the internal wave discussion, we consider perturbation equations with the background hydrostatic balance (31) subtracted. In this case, we will first make the equations dimensionless and conduct an asymptotic analysis to simplify the equations.

Guided by observation, we will assume that the wave motion has a characteristic horizontal velocity $\tilde{U}$ and horizontal length scale $\tilde{L}$. The characteristic time scale is long (weeks to months) compared to Earth's angular rotation rate, i.e. $\tilde{\omega} \sim \tilde{U}/\tilde{L} << \tilde{f}$. Moreover, we will assume that the vertical scale $\tilde{H} << \tilde{L}$ is small compared to the horizontal scale, with $\tilde{W} \sim \tilde{H}\tilde{U}/\tilde{L}$. This is because the motion has horizontal scales that are much larger than the depth of the ocean (only ≈ 5000 m). The assumption that $Ro = \tilde{U}/\tilde{f}\tilde{L} << 1$, where Ro is known as the *Rossby number*, is the crucial one. The resulting equations in dimensionless variables (denoted by a hat, e.g. $\tilde{U}\hat{u} = u$) are given by:

$$Ro\left(\frac{\partial \hat{\mathbf{u}}_\mathbf{H}}{\partial \hat{t}} + \hat{\mathbf{u}} \cdot \nabla \hat{\mathbf{u}}_\mathbf{H}\right) + \hat{\mathbf{f}} \times \hat{\mathbf{u}}_\mathbf{H} = -\nabla_H \hat{p}, \tag{43}$$

$$\frac{RoH}{L}\left(\frac{\partial \hat{w}}{\partial \hat{t}} + \hat{\mathbf{u}} \cdot \nabla \hat{w}\right) + \frac{\partial \hat{p}}{\partial \hat{z}} = \hat{b}, \tag{44}$$

$$Ro\left(\frac{\partial \hat{b}}{\partial \hat{t}} + \hat{\mathbf{u}} \cdot \nabla \hat{b}\right) + \hat{w}Bu = 0, \tag{45}$$

$$\nabla \cdot \hat{\mathbf{u}} = 0, \tag{46}$$

where $Bu = \tilde{N}^2\tilde{H}^2/\tilde{f}_0^2\tilde{L}^2$ is known as the Burger number (it is a measure of the significance of stratification compared with rotation in the dynamics). The buoyancy b and pressure p are scaled so that the dominant force balance is hydrostatic and geostrophic. *Geostrophic balance*,

$$\mathbf{f} \times \mathbf{u}_\mathbf{H} = -\nabla_H p, \tag{47}$$

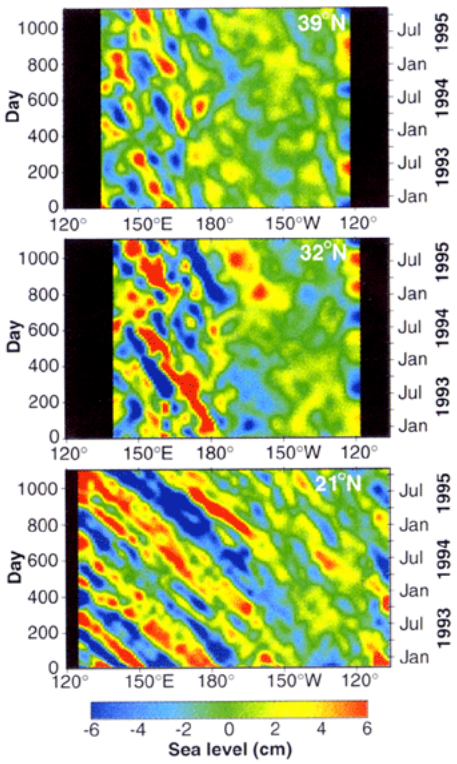

Figure 14: Time-longitude sections of filtered sea level in the Pacific Ocean along 39° N, 32°, and 21° N. From Chelton and Schlax (1996), *Global observations of oceanic Rossby waves.*

is a balance between the Coriolis force and lateral pressure gradient. It is the dominant force balance for large scale atmospheric and oceanic flows that are strongly constrained by Earth's rotation. And, because Rossby waves have large horizontal length scales and small timescales (that is to say low Rossby numbers $Ro << 1$), geostrophic balance is the zeroth order description of Rossby wave motion. Furthermore, because the motion has large horizontal scales, I allow for a spatially variable planetary rotation rate (the Coriolis frequency f can be called a *vorticity* since f is twice the local angular rotation rate and equal to the absolute vorticity in *solid body rotation*):

$$\mathbf{f} = (f_0 + \beta y)\mathbf{k}. \tag{48}$$

However, we will assume that $\tilde{\beta} \sim \tilde{U}/\tilde{L}^2$ (beta only varies by a small amount with y) so that

$$\hat{f} = \hat{f}_0 + Ro\hat{\beta}\hat{y}. \tag{49}$$

1.5.1 Asymptotic Expansions

To rigorously derive the wave equations, expand all the non-dimensional variables in Rossby number:

$$\hat{\mathbf{u}} = \hat{\mathbf{u_0}} + Ro\hat{\mathbf{u}}_\mathbf{1} + ... \tag{50}$$
$$\hat{p} = \hat{p_0} + Ro\hat{p_1} + ... \tag{51}$$
$$\hat{b} = \hat{b_0} + Ro\hat{b_1} + ... \tag{52}$$
$$\tag{53}$$

Substituting these expansions into the momentum equations yields at lowest order in Rossby number:

$$\hat{\mathbf{f_0}} \times \hat{\mathbf{u_0}} = -\nabla\hat{p}_0, \tag{54}$$

geostrophic balance. This flow is horizontally non-divergent and the vertical velocity is everywhere equal to zero. The buoyancy equation is just

$$\hat{w_0}Bu = 0. \tag{55}$$

At first order, the horizontal momentum equations are

$$\frac{\partial\hat{\mathbf{u_{0H}}}}{\partial\hat{t}} + \hat{\mathbf{u_{0H}}} \cdot \nabla\hat{\mathbf{u_{0H}}} + \hat{\beta}\hat{y}\hat{\mathbf{k}} \times \hat{\mathbf{u_0}}_H + \hat{\mathbf{f}} \times \hat{\mathbf{u_{1H}}} = -\nabla_H\hat{p_1}, \tag{56}$$

and the buoyancy evolution equation is

$$\frac{\partial\hat{b_0}}{\partial\hat{t}} + \hat{\mathbf{u_0}} \cdot \nabla\hat{b}_0 + \hat{w_1}Bu = 0. \tag{57}$$

Finally, the continuity equation at first order is just

$$\frac{\partial\hat{u_1}}{\partial\hat{x}} + \frac{\partial\hat{v_1}}{\partial\hat{y}} + \frac{\partial\hat{w_1}}{\partial\hat{z}} = 0 \tag{58}$$

These governing equations are time dependent and support Rossby waves.

1.5.2 Potential Vorticity: The path to a single governing equation

Now, the aim is to derive a single governing wave equation. This can be done in two steps: 1) by computing the evolution equation for vertical component of vorticity at lowest order: $\zeta_0 = \partial v_0/\partial x - \partial u_0/\partial y$[5] (and using continuity) to obtain:

$$\frac{\partial\hat{\zeta_0}}{\partial\hat{t}} + \hat{\mathbf{u_0}} \cdot \nabla\hat{\zeta_0} + \hat{v_0}\hat{\beta} = \hat{f}_0\left(\frac{\partial\hat{w_1}}{\partial\hat{z}}\right) \tag{59}$$

Differentiating the buoyancy equation with respect to z and substituting to eliminate $\hat{w}_1$ yields:

$$\frac{D_0(\hat{\zeta_0} + \hat{f})}{D\hat{t}} = -\hat{f}_0\frac{D_0}{D\hat{t}}\left(\frac{\partial}{\partial\hat{z}}\left(\frac{\hat{b}_0}{Bu}\right)\right) \tag{60}$$

[5]Note that in future sections of this document ζ denotes a vertical parcel displacement distance. In this section only, it represents the vertical component of relative vorticity.

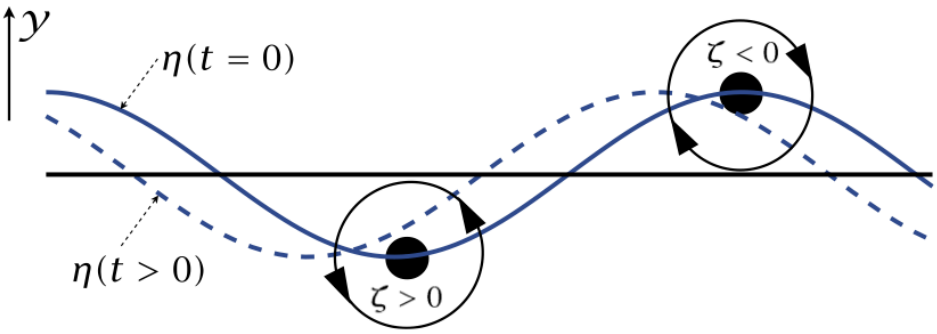

Fig. 5.4 The mechanism of a two-dimensional (x-y) Rossby wave. An initial disturbance displaces a material line at constant latitude (the straight horizontal line) to the solid line marked $\eta(t = 0)$. Conservation of potential vorticity, $\beta y + \zeta$, leads to the production of relative vorticity, as shown for two parcels. The associated velocity field (arrows on the circles) then advects the fluid parcels, and the material line evolves into the dashed line. The phase of the wave has propagated westwards.

Figure 15: A schematic illustrating how potential vorticity conservation leads to an oscillatory wave form. From Vallis (2006), *Atmospheric and Oceanic Fluid Dynamics*.

where $D_0/D\hat{t} = \partial/\partial\hat{t} + \hat{\mathbf{u}}_\mathbf{0} \cdot \nabla$ and we have interchanged $D_0/D\hat{t}$ and $\partial/\partial\hat{z}$ because the the vertical shear and horizontal buoyancy gradient are orthogonal at zeroth order (as implied by the geostrophic and hydrostatic balance, which together are known as the *thermal wind balance*; see Section 5.4.2 of Vallis (2006) *Atmospheric and Oceanic Fluid Dynamics* for a more complete presentation). We also use the zeroth order geostrophic balance to replace the buoyancy with pressure so that

$$\frac{D_0}{D\hat{t}}\left[\hat{\zeta}_0 + \hat{f} + \hat{f}_0\left(\frac{\partial}{\partial\hat{z}}\left(\frac{1}{Bu}\frac{\partial\hat{p}_0}{\partial\hat{z}}\right)\right)\right] = 0. \tag{61}$$

To obtain the final result, define a stream function that enforces horizontal non-divergence,

$$\frac{\partial\hat{\psi}}{\partial\hat{y}} = -\hat{u}, \tag{62}$$

$$\frac{\partial\hat{\psi}}{\partial\hat{x}} = \hat{v}. \tag{63}$$

$$\tag{64}$$

Introducing the stream function and using geostrophic balance to replace $\hat{p}$ with $\hat{\psi}$ ($\hat{f}_0\hat{\psi} = \hat{p}_0$) yields

$$\frac{D_0}{D\hat{t}}\left[\Delta\hat{\psi}_0 + \hat{\beta}\hat{y} + \hat{f}_0{}^2\left(\frac{\partial}{\partial\hat{z}}\left(\frac{1}{Bu}\frac{\partial\hat{\psi}_0}{\partial\hat{z}}\right)\right)\right] = 0. \tag{65}$$

The dimensional equation is:

$$\frac{Dq}{Dt} = 0, \tag{66}$$

$$q = \Delta\psi + f_0 + \beta y + f_0^2\frac{\partial}{\partial z}\left(\frac{1}{N^2}\frac{\partial\psi}{\partial z}\right), \tag{67}$$

where q is known as the *quasi-geostrophic potential vorticity* (one might think of this as a thickness weighted vorticity, see Figure 16). Top and bottom boundary conditions are required for ψ. Here, I assume the top and bottom are free-slip, flat, and rigid. See Vallis (2006) or Pedlosky (1986) for extensions to other circumstances, including the addition of mechanical forcing at the boundary, rough topography, and/or buoyancy sources and sinks etc. In the simple rigid lid case, the boundary conditions can be derived from the buoyancy equation at the top and bottom surfaces,

$$\frac{Db'}{Dt} = 0. \tag{68}$$

Geostrophic and hydrostatic balance imply that

$$b' = f_0 \frac{\partial \psi}{\partial z}, \tag{69}$$

which yields a boundary condition for ψ.

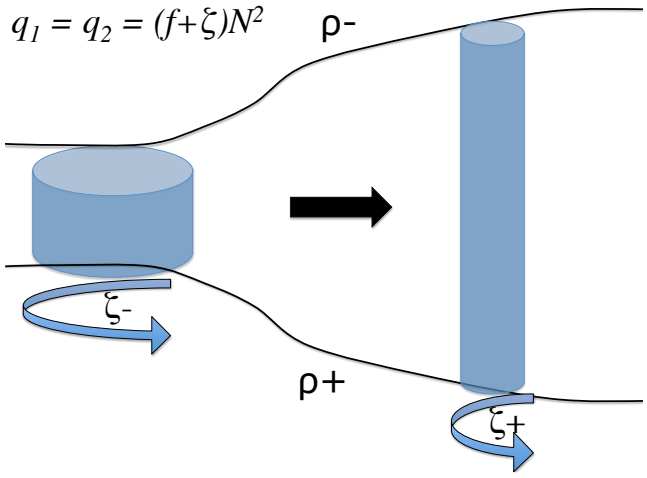

Figure 16: A schematic illustrating the potential vorticity conservation law. *Potential vorticity* (PV) is an isopycnal-layer-thickness weighted vorticity, and in a more general form it is defined as $\omega_{\mathbf{a}} \cdot \nabla b$ where $\omega_{\mathbf{a}}$ is the absolute vorticity vector (e.g. all components of planetary (f) + relative (ζ) vorticity). In the case of the *quasi-geostrophic* asymptotic limit, horizontal vorticity components are neglected in the PV, and q reduces to $(f + \zeta)N^2$ where ζ is the vertical component of the relative vorticity in this context, $\zeta = \mathbf{k} \cdot (\nabla \times \mathbf{u})$.

1.5.3 Ducted Quasi-Geostrophic Rossby waves

As in the discussion of ducted internal waves, we linearize the governing equations to obtain

$$\frac{\partial}{\partial t}\left(\Delta\psi + f_0^2 \frac{\partial}{\partial z}\left(\frac{1}{N^2}\frac{\partial \psi}{\partial z}\right)\right) + \beta \frac{\partial \psi}{\partial x} = 0 \tag{70}$$

and look for ducted solutions of the plane wave form:

$$\psi = Re(\psi_0(z) e^{i(kx+ly-\omega t)}). \tag{71}$$

Inserting this ansatz into (67) yields

$$\left(\beta k + \omega K^2\right) \psi_0(z) = \omega \frac{\partial}{\partial z} \left(\frac{f_0^2}{N^2(z)} \frac{\partial \psi_0(z)}{\partial z} \right), \tag{72}$$

where $K = \sqrt{k^2 + l^2}$ is the magnitude of the horizontal wave vector.

If we assume N is constant, and that $\partial\psi/\partial z = 0$ at the top and bottom, then the solutions are given by $\cos(mz)$, where $m = j\pi/D$ with $j = 1, 2, ...$ a natural number and D the depth of the ocean. In that case,

$$\omega = \frac{-\beta k}{K^2 + m^2 \frac{f^2}{N^2}}. \tag{73}$$

A similar dispersion relation holds with arbitrary vertical wavenumber m for free wave solutions (as opposed to quantized m for ducted wave solutions), similar to the internal wave solution.

However, otherwise, the Rossby wave dispersion relation is quite different from that for internal waves. It depends crucially the strength of the planetary vorticity gradient, $\beta = \partial f/\partial y$. Moreover, because $\beta \geq 0$, the zonal *phase speed*, the speed at which wave crests propagate ω/k, is always from east to west (as in Figure 14).

Let's make a back-of-the-envelope estimate for the phase speed of a low-mode baroclinic Rossby wave. For 20^o N, $\beta \approx 2 \times 10^{-11}$ s^{-1} m^{-1}, $m \approx 2\pi/5000$ m^{-1}, and $f_0^2/N^2 \approx 10^{-4}$. This results in a phase speed of about 10 km per day, which is a fairly good approximation of the phase speed observed in Figure 14 (C) given the crudeness of our estimates used in the calculation.

1.6 Lagrangian/Conservation-Law Perspectives

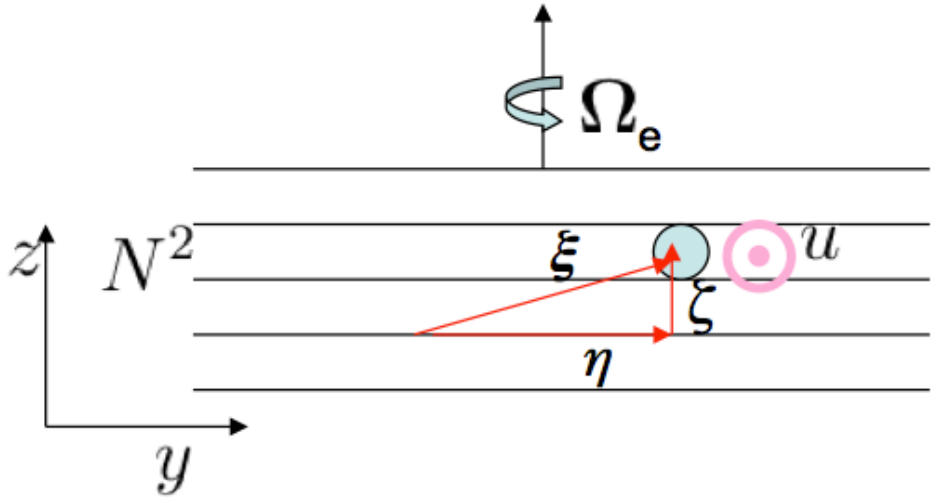

Figure 17: A schematic illustrating the parcel displacement $\boldsymbol{\xi} = (\xi, \eta, \zeta)$ in (x, y, z) in a motionless fluid rotating at angular frequency Ω_e stratified with constant buoyancy frequency N. Modified from Leif Thomas.

The derivation of the quasi-geostrophic potential vorticity conservation equation and Rossby wave solutions in continuous stratification demonstrates the power of a conservation law. Rossby waves (and a great deal more of oceanic and atmospheric dynamics) can be interpreted entirely in terms of this one equation (see e.g. Hoskins et al. 1985, *On the use and significance of isentropic potential vorticity maps* for a detailed discussion, and Hoskins 2015, *Potential vorticity and the PV perspective* for a brief, not-particularly-technical summary of Brian Hoskins' personal perspective). Figure 15 demonstrates how conservation of potential vorticity (or vorticity in a homogeneous layer) results in a westward propagating Rossby wave. But, this is just a subtle hint at the remarkable power of this one conservation law.

Motivated by these results, I briefly describe a simple Lagrangian parcel interpretation of internal wave motions. Consider the perturbation of a Lagrangian fluid parcel in a rotating stratified fluid (see Figure 17). Assuming that the motion adapts immediately to the background pressure field (as it does in the plane wave solutions above, where the pressure gradient force is always perpendicular to parcel velocities), we can rewrite the governing equations in terms of Lagrangian conservation laws for absolute momentum and buoyancy,

$$\frac{DM_x}{Dt} = 0, \tag{74}$$

$$\frac{DM_y}{Dt} = 0, \tag{75}$$

$$\frac{Dw}{Dt} = b', \tag{76}$$

$$\frac{Db}{Dt} = 0, \tag{77}$$

where $M_x = u(x,y,z,t) - f\eta$ is conserved, $M_y = v(x,y,z,t) + f\xi$ is conserved, and $b = b'(x,y,z,t) + \overline{b}(z)$ is conserved. Here, $D\zeta/Dt = w$, $D\eta/Dt = v$ and $D\xi/Dt = u$. These results imply the parcel experiences restoring forces as a function of displacement, that can be written in simple form:

$$F_x = \frac{Du}{Dt} = +fv = -f^2\xi, \tag{78}$$

$$F_y = \frac{Dv}{Dt} = -fu = -f^2\eta, \tag{79}$$

$$F_z = \frac{Dw}{Dt} = b' = -N^2\zeta, \tag{80}$$

where I have assumed (without loss of generality) that $M_x = M_y = 0$. From these coupled equations for the forces on the parcel as a function of position $\boldsymbol{\xi} = (\xi, \eta, \zeta)$, one can derive a single Lagrangian oscillator equation for the magnitude of the displacement $|\boldsymbol{\xi}|$ at angle $\theta = \tan^{-1}(\sqrt{|\xi|^2 + |\eta|^2}/|\zeta|)$

$$\frac{D^2|\boldsymbol{\xi}|}{Dt^2} = -f^2|\boldsymbol{\xi}_H|\cos(\theta) - N^2|\zeta|\sin(\theta) = -|\boldsymbol{\xi}|\left(f^2\cos^2(\theta) + N^2\sin^2(\theta)\right). \tag{81}$$

Assuming simple harmonic motion in time yields the dispersion relation,

$$\boxed{\omega^2 = f^2\cos^2(\theta) + N^2\sin^2(\theta),} \tag{82}$$

which is identical to (42) and highlights the fact that internal waves radiate in a cone (with angle θ from horizontal) from a source oscillating at a fixed frequency in a medium with constant stratification and constant f, as mentioned above (see Figure 12).

1.7 Waves in an inhomogeneous medium

Now that we have covered the basic properties of surface gravity waves, internal waves and Rossby waves in a uniform medium, I'd like to discuss how to extend the ideas to a non-uniform medium because these ideas will play an important role in my lecture tomorrow.

The idea is to generalize the discussion of plane waves above to allow for an inhomogeneous medium and inhomogeneous wave field that locally look like plane waves. Therefore, we will consider solutions of the form

$$\psi = Re(\psi_0(x,y,z,t)e^{i(\alpha(x,y,z,t)}), \tag{83}$$

where the characteristic length and time scales of the *envelope or amplitude function* (ψ_0), which I denote L_A and T_A, are much greater than the wavelength and period of the oscillation, λ and $2\pi/\omega$ respectively (see e.g. Figure 18).

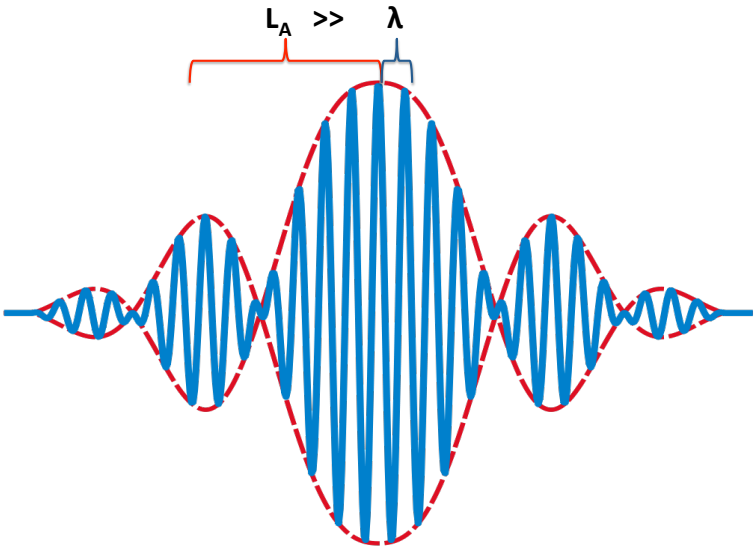

Figure 18: A schematic of a wave with a modulated amplitude. The envelope function varies on a scale much larger than the wavelength, $L_A >> \lambda$. Modified from Wikipedia.

The the wavenumber vector and frequency are defined by

$$\mathbf{k} = (k,l,m) = \nabla\alpha, \tag{84}$$

$$\omega = -\frac{\partial\alpha}{\partial t}. \tag{85}$$

A consequence of the definition is that

$$\frac{\partial \mathbf{k}}{\partial t} + \nabla\omega = 0, \tag{86}$$

assuming ω and $\mathbf{k}$ are varying slowly in space and time.

I now define a general dispersion relation,

$$\omega = \Omega(\mathbf{k}, \mathbf{x}, t), \tag{87}$$

which is locally equivalent to the dispersion relation in a constant medium, but varies slowly in time and space. Then, by the chain rule

$$\frac{\partial \omega}{\partial t} = \frac{\partial \Omega}{\partial t} + \frac{\partial \Omega}{\partial \mathbf{k}} \frac{\partial \mathbf{k}}{\partial t}, \tag{88}$$

$$= \frac{\partial \Omega}{\partial t} - \frac{\partial \Omega}{\partial \mathbf{k}} \nabla \omega \tag{89}$$

The first term on the right hand side results from a change in the dispersion relation (i.e. due to a change in the local medium at a given $\mathbf{x}$) as a function of time. The second term results from a change in wavenumber at a given location as a function of time. Therefore, we can reorder the terms as

$$\boxed{\frac{D_g \omega}{Dt} = \frac{\partial \omega}{\partial t} + \mathbf{c_g} \cdot \nabla \omega = \frac{\partial \Omega}{\partial t},} \tag{90}$$

where we have defined the *group velocity*,

$$\boxed{\mathbf{c_g} = \nabla_{\mathbf{k}} \Omega,} \tag{91}$$

and the wave equivalent of the material derivative, $D_g/Dt = \partial/\partial t + \mathbf{c_g} \cdot \nabla$, i.e. the Lagrangian derivative moving at the group velocity.

Returning to (86) we write

$$\frac{\partial \mathbf{k}}{\partial t} + \frac{\partial \Omega}{\partial \mathbf{x}} + \frac{\partial \Omega}{\partial \mathbf{k}} \frac{\partial \mathbf{k}}{\partial \mathbf{x}} = 0, \rightarrow \tag{92}$$

$$\boxed{\frac{D_g \mathbf{k}}{Dt} = \frac{\partial \mathbf{k}}{\partial t} + \mathbf{c_g} \cdot \nabla \mathbf{k} = -\nabla \Omega.} \tag{93}$$

To summarize, *moving with the group velocity,* the change in wavenumber is given by the explicit spatial gradient of the dispersion relation. Similarly, *moving with the group velocity*, the change in frequency is given by the explicit temporal derivative of the dispersion relation. In the absence of temporal and spatial gradients in the dispersion relation, the wave number and frequency are constant moving at the group velocity.

1.8 Conclusion and some other examples

I want to conclude by mentioning that there are many other prominent and extremely important examples of oceanic wave motion that I have not discussed. For example, every year instabilities along the equator produce a magnificent pattern of waves/vortices that propagate to the west along the equator with periods of several weeks (Figure 20). These are a fascinating breed of wave with great significance for equatorial mixing, the heat budget of the cold tongue, and other equatorial ocean processes. Moreover, I have totally neglected to discuss tides (see Figure 19), which are of central importance to coastal life and are also one of the most prominent sources of energy for internal waves in the ocean (tides generate internal waves by sloshing over mid ocean ridges).

For the wave motions I have discussed, classic linear water waves, internal waves, and Rossby waves, the discussion has focused on the derivation of the governing equations and the properties of plane-wave and ducted solutions. There is a great deal to be learned by investigating the dynamics of these waves in situations of practical interest, as even the most cursory search of the research

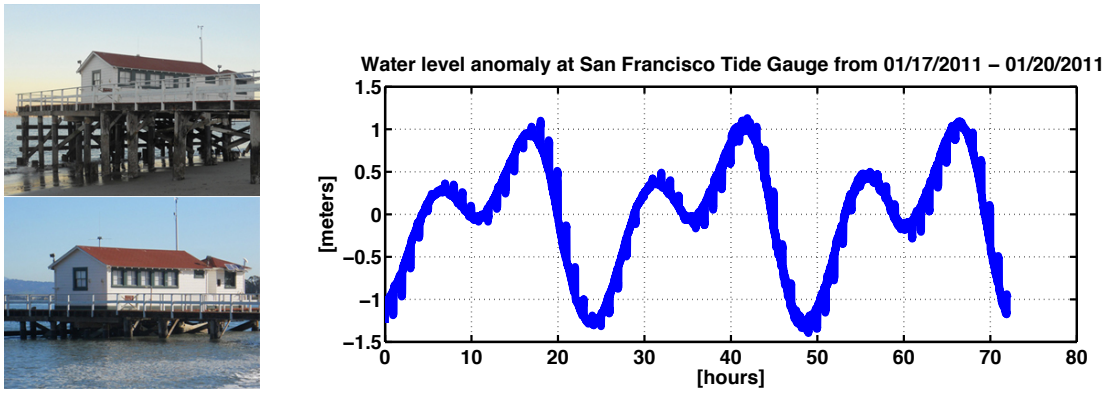

Figure 19: (Left) Photos showing the difference between high and low tide in San Francisco. (Right) Data from the tide gauge showing the time evolution of the water height anomaly associated with the tidal oscillations.

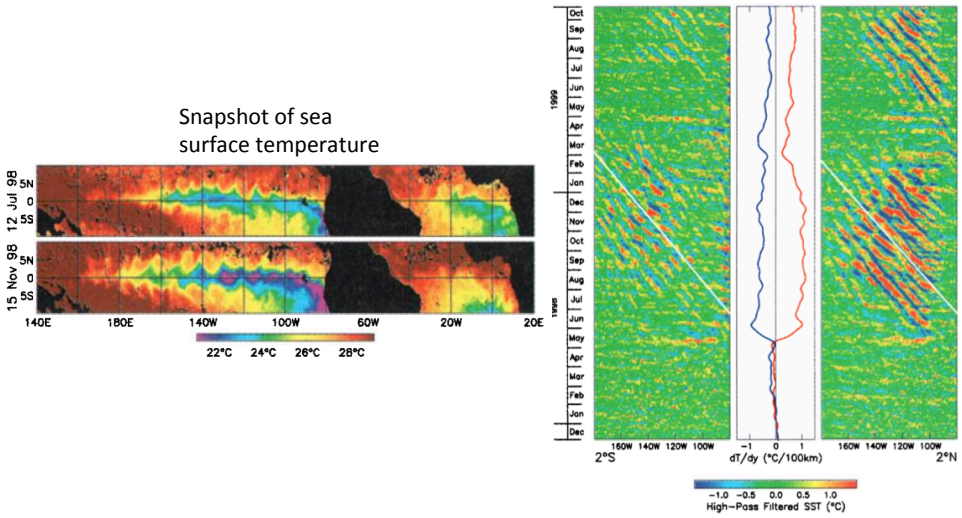

Figure 20: A snapshot (left) and time-longitude plots along 2° N and 2° S (right) of sea surface temperature in the tropical Pacific. From Chelton et al. (2000), *Satellite microwave SST observations of transequatorial tropical instability waves.*

literature on these topics will quickly demonstrate. Two principle practical problems include: 1) non-linearity (i.e. large amplitude) of the wave motion invalidates the assumptions employed here, 2) inhomogeneity of the medium. I will discuss the later issue in more detail during tomorrow's lecture.

2 Internal wave propagation in an inhomogeneous ocean

The second of two lectures to be delivered at Capital Normal University, Beijing
March 30-April 3, 2015

In my previous lecture, I introduced several different classes of ocean wave. That discussion focused on wave motions in a homogeneous medium, or a medium with vertically varying buoyancy frequency N. Of course, the real ocean (like most other geophysical fluids) is far from homogeneous and methods must be employed to understand how variations in the medium (e.g. variations in depth, mean current, stratification etc.) modify the properties of all types of waves as they propagate. This discussion will build on the ideas presented in my first lecture by giving a more in-depth introduction to some of the tools that have been developed to analyze oceanic wave motions in an inhomogeneous medium. The discussion will be exclusively in terms of internal waves today, but the ideas can be applied to other classes of wave motion such as Rossby waves or surface waves, among others. This perspective is merely a reflection of my recent research, in which internal waves play a central role.

2.1 Internal wave energetics

Yesterday, I showed that there is significant internal wave energy in the ocean. Moreover, I showed that internal waves tend to exhibit a continuous energy spectrum with decreasing energy at higher frequency (and wavenumber) and peaks in energy at certain particular frequencies (Figure 9). For example, the North Pacific tends to exhibit elevated internal wave energy at semi-diurnal frequencies and long vertical length scales (low vertical wavenumber) as suggested by Figure 7. The question that motivates this lecture is: *what is the source of the observed internal wave energy* (both the dominant semi-diurnal wave, as well as the rest of the frequency/wavenumber spectrum)? Did the wave energy propagate from a great distance to that location? How does that energy ultimately dissipate? Is it a local process in the ocean interior or does it occur at boundaries? In short, I'd like to know more about the *life cycle* of the internal wave, which might be separated into three phases: generation (energy injection into the wave field), propagation (energy transfers within the wave field, in the space, frequency, and wavenumber domains), and dissipation (irreversible loss of energy from the internal wave field).[6] A similar approach is useful for other classes of wave motion, but we will not pursue such an investigation here.

To address this question, we must derive the appropriate internal wave energy equation. The procedure is as follows: multiply the momentum equations by velocity and the buoyancy equations by b/N^2 and add the resulting equations to obtain,

$$\frac{\partial E}{\partial t} = -\nabla \cdot (p\mathbf{u}), \tag{94}$$

[6] In fact, it is difficult to precisely define whether or not perturbation energy is in the "internal wave field." Clearly internal wave motions must approximately satisfy the basic properties (e.g. dispersion relation, frequency range $f \leq \omega \leq N$) discussed in yesterday's lecture. However, the assumptions of that simple model do not hold exactly. Although certain *approximate* decompositions can be made on the basis of the assumptions used to derive the respective reduced models, it remains unclear if a general decomposition between internal wave motions and other classes (e.g. Rossby waves) is possible.

where

$$E = KE + PE = \frac{\rho_0}{2}\left(|\mathbf{u}|^2 + b^2/N^2\right) \tag{95}$$

and the right hand side of (94) is known as the *energy flux divergence*. Studying this equation is particularly easy when the solution is that of a pure plane wave, e.g. $\psi = Re(\psi_0 e^{i(ly+mz-\omega t)})$ and we assume (without loss of generality) that the wave vector is oriented in the y, z plane, i.e. $k = 0$.[7] One can explore the relationship between variables by reformulating the governing equations into an algebraic system of 5 equations with 8 variables:

$$\begin{aligned}
-i\omega u - fv &= 0, && (96)\\
-i\omega v + fu + ilp/\rho_0 &= 0, && (97)\\
-i\omega w + imp/\rho_0 - b &= 0, && (98)\\
-i\omega b + N^2 w &= 0, && (99)\\
imw + ilv &= 0. && (100)
\end{aligned}$$

Factoring out the dynamical variables results in a dispersion relation (42), which relates l and m to ω. Given the amplitude and phase of one dynamical variable, let's say $v = Re(v_0 e^{i(ly-\omega t)})$ for example, as well as the frequency (or aspect ratio l/m, which is equivalent to frequency via the dispersion relation), one can derive formulas for all the other dynamical variables,

$$\begin{aligned}
u &= \frac{ifv}{\omega}, && (101)\\
w &= -\frac{lv}{m}, && (102)\\
b &= \frac{ilvN^2}{m\omega}, && (103)\\
p/\rho_0 &= \frac{-lv}{m^2\omega}\left(\omega^2 - N^2\right), && (104)\\
\eta &= \frac{iv}{\omega}, && (105)\\
\zeta &= \frac{-ilv}{m\omega}, && (106)
\end{aligned}$$

where η and ζ are parcel displacements in the y and z directions, respectively. Together, these are known as *polarization relations*. In this case, u, b are in phase while p, v and w are in quadrature (i.e. orthogonal to u and b and in phase with each other).

Now, use the Lagrangian relationships derived in the previous lecture (i.e. $f^2\eta^2 = u^2$ and $N^4\zeta^2 = b^2$ to write

$$\begin{aligned}
E &= \frac{\rho_0}{2}\left(v^2 + w^2 + f^2\eta^2 + N^2\zeta^2\right),\\
&= \frac{\rho_0}{2}\left(|\mathbf{u}|^2 + |\boldsymbol{\xi}|^2(f^2\cos^2(\theta) + N^2\sin^2(\theta)\right) = \frac{\rho_0}{2}\left(|\mathbf{u}|^2 + |\boldsymbol{\xi}|^2\omega^2\right), && (107)
\end{aligned}$$

where η and ζ are parcel displacements in the y, z plane (see Figure 17, $|\boldsymbol{\xi}| = \sqrt{\eta^2 + \zeta^2}$, $\theta = \tan^{-1}(\zeta/\eta)$, $|\mathbf{u}| = \sqrt{v^2 + w^2}$). This is the energy equation associated with (81). Writing the energy

[7] We can always rotate the coordinate system horizontally to achieve this.

this way makes it explicit that b^2/N^2 is a potential energy. Moreover, it is also clear that this is an harmonic oscillator equation with frequency ω (42). Furthermore, writing the energy equation this way highlights the conservative nature of the internal wave equations and, in particular, shows that the internal wave system is of *Hamiltonian* form,[8] which implies that there is an energy equipartition, e.g.

$$\begin{aligned}\langle v^2+w^2\rangle &= \frac{|v_0|^2}{2}\left(1+\frac{l^2}{m^2}\right)=\frac{|v_0|^2}{2}\left(\frac{m^2+l^2}{m^2}\right)\\ &= \frac{|v_0|^2}{2}\left(\frac{fm^2+N^2l^2}{\omega^2m^2}\right)=\langle f^2\eta^2+N^2\zeta^2\rangle\end{aligned} \tag{108}$$

where $\langle\rangle=\frac{1}{T}\int_0^T dt$ with $T=2\pi/\omega$ is a wave-period average.

The wave-period averaged energy fluxes are given by

$$\langle p\mathbf{u}\rangle=\langle(0,pv,pw)\rangle=\left(\frac{-\rho_0 l|v_0|^2(\omega^2-N^2)}{2m^2\omega}\right)\left(1,-\frac{-l}{m}\right), \tag{109}$$

where $T=2\pi/\omega$, the angle brackets denote the same wave period averaging operator. Now, I'd like to propose that this plane wave flux is equal to the energy density times the group velocity (91), i.e.

$$\langle p\mathbf{u}\rangle=\langle E\mathbf{c_g}\rangle. \tag{110}$$

Let's check. Using (91), find that

$$(c_{gy},c_{gz})=\left(\frac{\partial\omega}{\partial l},\frac{\partial\omega}{\partial m}\right)=\left[\frac{l}{\omega}\left(\frac{N^2-\omega^2}{l^2+m^2}\right),\frac{m}{\omega}\left(\frac{f^2-\omega^2}{m^2+l^2}\right)\right]. \tag{111}$$

Then, by the equipartition result (108),

$$\langle E\rangle=\frac{\rho_0|v_0|^2}{2}\left(\frac{m^2+l^2}{m^2}\right). \tag{112}$$

Together,

$$\langle E\rangle(c_{gy},c_{gz})=\frac{\rho_0|v_0|^2}{2m\omega}\left[\frac{l}{m}\left(N^2-\omega^2\right),\left(f^2-\omega^2\right)\right] \tag{113}$$

Using

$$\left(\omega^2-f^2\right)m^2=(N^2-\omega^2)l^2, \tag{114}$$

which is derived from the dispersion relation (42), it is clear that indeed

$$\langle\mathbf{u}p\rangle=\langle E\rangle\mathbf{c_g} \tag{115}$$

for the plane internal waves.

As a result, we finally see one of the most important properties of the *group velocity* in a wave field that varies slowly in time and space:

$$\boxed{\frac{\partial\langle E\rangle}{\partial t}+\nabla\cdot(\mathbf{c_g}\langle E\rangle)=0\rightarrow\frac{D_g\langle E\rangle}{Dt}=-\langle E\rangle\nabla\cdot\mathbf{c_g}.} \tag{116}$$

[8]See e.g. Meyer et al. 2009, *Introduction to Hamiltonian Dynamical Systems*, Rainville and Pinkel (2005), *Propagation of low mode internal waves through the ocean*, or Salmon 1983, *Practical use of Hamilton's principle.*

In a plane-wave, the energy flux is non-zero, but the wave-period average energy flux *divergence* is zero. However, in a slowly varying wave field (see Figure 18), this equation describes how the wave amplitude evolves in space and time. I note that although I derived this result for internal waves, the concept applies to any type of wave field that looks like a slowly varying plane wave.

Some final points to note (and check):

1. The group velocity runs parallel to *characteristics* of the governing equations.
2. Lines of constant wave phase are parallel to the characteristics and the group velocity. Hence, internal wave phase propagates perpendicular to internal wave energy.

2.1.1 Example: Ray tracing and turning depths

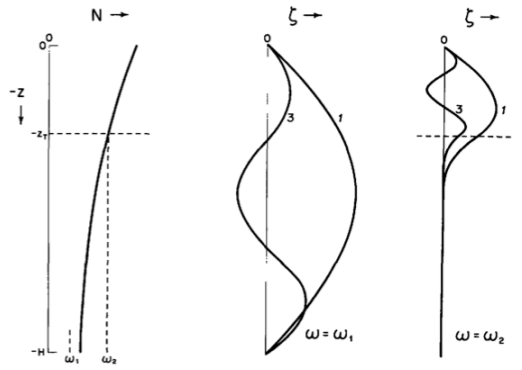

Figure 9.8 Vertical displacements $\zeta(z)$ in a variable-N ocean, for modes $j = 1$ and $j = 3$. ω_1 is taken to be less than $N(z)$ at all depths. ω_2 is less than $N(z)$ in the upper oceans above $z = -z_p$ only.

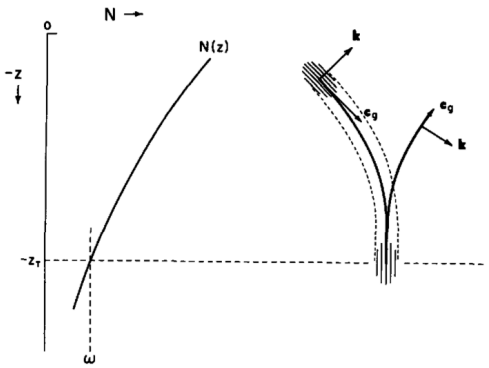

Figure 9.9 Propagation of a wave packet in a variable-$N(z)$ ocean without shear (U = constant). The turning depth z_T occurs when $\omega = N(z_T)$.

Figure 21: Two figures from Munk's *Internal waves and small scale processes* illustrating some of the properties of internal waves in an ocean with vertically-varying buoyancy frequency N. (Left) the first three vertical modes of vertical displacement ζ when $\omega < \min[N(z)]$ and the first three modes when $\omega = N(-z_T)$ where $-z_T$ is known as a turning depth. (right) the propagation of a wave packet with frequency $\omega = N(-z_T)$ toward the turning depth.

Ray tracing is a tool that can be employed to investigate wave propagation in a hyperbolic system of governing equations with variable coefficients and has applications far beyond ocean science (e.g. to optics, acoustics, etc.). The basic assumptions are similar to those used to derive the group velocity in Section 1.7 and the above energy evolution equation (116). A quick example can illustrate ray tracing in action.

Consider waves in an ocean with exponentially increasing $N(z) \propto e^{Az}$ for some A with increasing depth off the bottom as shown in the left-most panel of Figure 21. When the wave motion has a frequency $\omega < N(z)$ for all depths z, the vertical mode number m, given by (40) is non-zero for all z and the vertical mode structure is not substantially different from an ocean with constant N (also see Figure 10). However, in an ocean with variable $N(z)$, the wave energy may be excluded from any depth z where $\omega > N(z)$. Where $m(z) = 0$, i.e. where $\omega = N(z)$ in (40), the governing

equation changes from hyperbolic to elliptic form. Consequently, the vertical structure function is an *Airy function* (see the textbook by Bender and Orszag, *Advanced mathematical methods for scientists and engineers*).

In a more heuristic approach one can use the approximation that

$$\nabla \cdot \langle E \rangle \mathbf{c_g} = 0 \rightarrow \frac{\partial \langle E \rangle c_{gz}}{\partial z} = 0 \tag{117}$$

together with the evolution equation for m (93), to consider the propagation of a *wave packet*, a small envelope of non-zero wave amplitude as shown in Figure 21.

2.2 Example: Waves propagating perpendicular to a baroclinic mean current

We now extend (116) to investigate near-inertial internal waves (ω near f) propagating *perpendicular* to a flow with spatially variable velocity $u_g(y,z)$ and spatially variable background stratification $b_g(y,z)$. The background flow is in geostrophic and hydrostatic balance, that is

$$f\frac{\partial u_g}{\partial z} = -\frac{\partial b_g}{\partial y}. \tag{118}$$

This formula, which relates the vertical gradient in velocity to the horizontal gradient in buoyancy is known as the *thermal wind* equation.

If we consider internal waves as small perturbations to a steady background state that is in thermal wind balance (as opposed to merely hydrostatic balance in earlier discussions), we obtain the following linearized governing equations for hydrostatic internal waves propagating perpendicular to a mean current,

$$\frac{\partial u_a}{\partial t} + v_a\frac{\partial u_g}{\partial y} + w_a\frac{\partial u_g}{\partial z} - fv_a = 0, \tag{119}$$

$$\frac{\partial v_a}{\partial t} + fu_a = -\tfrac{1}{\rho_0}\tfrac{\partial p_a}{\partial y}, \tag{120}$$

$$0 = -\tfrac{1}{\rho_0}\tfrac{\partial p_a}{\partial z} + b_a, \tag{121}$$

$$\frac{\partial b_a}{\partial t} + v_a\frac{\partial b_g}{\partial y} + w_a\frac{\partial b_g}{\partial z} = 0, \tag{122}$$

$$\frac{\partial v_a}{\partial y} + \frac{\partial w_a}{\partial z} = 0, \tag{123}$$

where the subscript a denotes the time-dependent perturbation and the subscript g denotes the steady background. Then we obtain the following modified wave equation for ψ (where $v_a = \partial\psi/\partial z$ and $w_a = -\partial\psi/\partial y$),

$$\left[F^2 + \frac{\partial^2}{\partial t^2}\right]\frac{\partial^2\psi}{\partial z^2} + 2S^2\frac{\partial^2\psi}{\partial z\partial y} + N^2\frac{\partial^2\psi}{\partial y^2} = 0, \tag{124}$$

where $F^2 = f\left(f - \frac{\partial u_g}{\partial y}\right)$, $S^2 = f\frac{\partial u_g}{\partial z} = -\frac{\partial b_g}{\partial y}$, and $N^2 = \frac{\partial b_g}{\partial z}$ and all three depend on both y and z. The resulting dispersion relation is given by

$$\omega = \pm\sqrt{F^2 + 2S^2\frac{l}{m} + N^2\frac{l^2}{m^2}}. \tag{125}$$

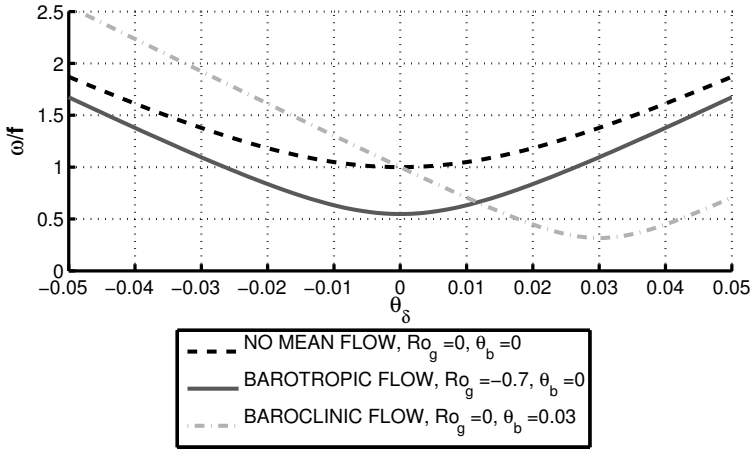

Figure 22: The frequency of oscillation of fluid parcels displaced at an angle θ with respect to the horizontal, for a basic state without a background flow ($Ro_g = 0$, $Ri_g = \infty$, dashed), with a barotropic flow ($Ro_g = -7/10$, $Ri_g = \infty$, solid) and with a baroclinic flow ($Ro_g = 0$, $Ri_g = 10/9$, dot-dashed). Baroclinicity both lowers the minimum frequency and shifts the angle, θ, where this occurs to coincide with the angle that isopycnals make with the horizontal.

An important result is that the minimum frequency is no longer the Coriolis frequency, f, but varies with space:

$$\omega_{\min} = \sqrt{F^2 - S^4/N^2} = \sqrt{\frac{fq}{N^2}} = f\sqrt{1 + Ro_g - Ri_g^{-1}}, \tag{126}$$

where $Ro_g = -\partial u_g/\partial y/f$ and $Ri_g = f^2N^2/S^4$ and q is the Ertel potential vorticity $(f - \partial u_g/\partial y)N^2 - S^4/f$. In the case that the argument of the minimum frequency is negative, the frequency becomes imaginary, which means that the flow is unstable. The fastest growing symmetric normal mode will be parallel to isopycnals and grow at the rate suggested by (126).

2.2.1 Lagrangian Perspective

If we consider a Lagrangian parcel displacement $\boldsymbol{\xi}$ in a baroclinic geostrophic flow (e.g. Figure 23), the forces are given by:

$$F_\xi = \frac{Du_a}{Dt} = fv_a = -f^2\xi, \tag{127}$$

$$F_\eta = \frac{Dv_a}{Dt} = -fu_a = f\nabla M_g \cdot \boldsymbol{\xi} = f\left(\eta\frac{\partial M_g}{\partial y} + \zeta\frac{\partial M_g}{\partial z}\right) = -F^2\eta + S^2\zeta, \tag{128}$$

$$F_\zeta = \frac{Dw_a}{Dt} = b_a = -\nabla b_g \cdot \boldsymbol{\xi} = -\zeta\frac{\partial b_g}{\partial z} - \eta\frac{\partial b_g}{\partial y} = -N^2\zeta + S^2\eta. \tag{129}$$

The following conservation laws have been employed (assuming the parcel adjusts instantaneously to the background pressure; this is analogous to the plane wave assumption, where the pressure

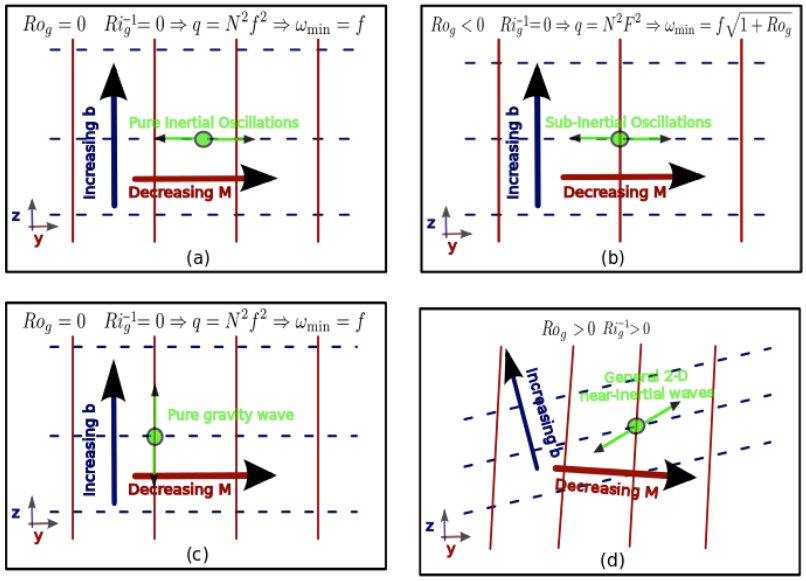

Figure 23: A series of 4 schematics illustrating different types of inertia-gravity wave oscillations. (A) a pure inertial oscillation in a motionless background, (B) a sub-inertial oscillation in a region of anti-cyclonic vorticity, (C) a pure gravity wave in a motionless background, and (D) a generalized inertia-gravity wave in a baroclinic background flow with both vertical velocity shear and a horizontal density gradient subject to the thermal wind balance, $f\partial u_g/\partial z = -\partial b_g/\partial y$, and possibly non-zero vertical relative vorticity ($Ro_g = \zeta_g/f$).

gradient force is always orthogonal to parcel velocities):

$$\frac{DM_x}{Dt} = 0, \tag{130}$$

$$\frac{DM_y}{Dt} = 0, \tag{131}$$

$$\frac{Db}{Dt} = 0, \tag{132}$$

where the absolute momenta are given by:

$$M_x = u_a + u_g - f\eta = u_a + M_g, \tag{133}$$

$$M_y = v_a + f\xi. \tag{134}$$

In this case, we can write

$$\frac{D^2|\boldsymbol{\xi}|}{Dt^2} = -|\boldsymbol{\xi}|\left(F^2\cos^2(\theta) - 2S^2\sin(\theta)\cos(\theta) + N^2\sin^2(\theta)\right) \tag{135}$$

which permits solutions of the form $\xi = Re(\hat{\xi}\exp(-i\omega t))$ where $\hat{\xi}$ is a complex amplitude. This yields frequencies

$$\begin{aligned}\omega &= \sqrt{F^2\cos^2(\theta) - 2S^2\sin(\theta)\cos(\theta) + N^2\sin^2(\theta)} \\ &\approx \sqrt{F^2 - 2S^2\theta + N^2\theta^2}. \end{aligned} \tag{136}$$

The dispersion relation is equivalent to that of (125) and is plotted for several example background flows in Figure 22. We can also derive a more general wave-period-averaged energy equation,

$$\begin{aligned}\frac{\partial\langle E\rangle}{\partial t} &= \frac{\rho_0}{4}\frac{\partial}{\partial t}\left[|\hat{v}_a|^2 + \left(F^2|\hat{\eta}|^2 - 2S^2\hat{\eta}\hat{\zeta}^* + N^2|\hat{\zeta}|^2\right)\right] = \frac{\rho_0}{2}\frac{\partial|\hat{v_a}|^2}{\partial t} \\ &= -\frac{1}{2}\nabla\cdot(\hat{p}_a\hat{\mathbf{u}}_a^*) = -\nabla\cdot(\mathbf{c_g}\langle E\rangle). \end{aligned} \tag{137}$$

Again, writing the energy this way makes it clear that the system is a conservative Hamiltonian system with an energy equipartition, e.g.

$$|\hat{v}_a|^2 = \left(F^2|\hat{\eta}|^2 - 2S^2\hat{\eta}\hat{\zeta}^* + N^2|\hat{\zeta}|^2\right). \tag{138}$$

One can check the energy equipartition using the dispersion relations,

$$\hat{u}_a = i\tfrac{\hat{v}_a}{\omega f}\left(F^2 + \tfrac{l}{m}S^2\right), \tag{139}$$

$$\hat{w}_a = -\tfrac{l}{m}\hat{v}_a, \tag{140}$$

$$\hat{b}_a = i\tfrac{\hat{v}_a}{\omega}\left(S^2 + \tfrac{l}{m}N^2\right), \tag{141}$$

$$\hat{p}_a = \tfrac{\rho_0\hat{v}_a}{m\omega}\left(S^2 + \tfrac{l}{m}N^2\right), \tag{142}$$

$$\hat{\eta}_a = \tfrac{i\hat{v}_a}{\omega}, \tag{143}$$

$$\hat{\zeta}_a = \tfrac{-il\hat{v}_a}{m\omega}, \tag{144}$$

and confirm the equivalence of the pressure work and group velocity times wave-averaged energy density using the group velocity equations,

$$\mathbf{c_g} = \nabla_{(l,m)}\omega = \frac{\left(S^2 + N^2\frac{l}{m}\right)}{\omega m}\left[1, -\frac{l}{m}\right]. \tag{145}$$

2.2.2 Ray Tracing and numerical simulation

Now, let's investigate how wave motion refracts through a model strongly baroclinic flow following the group velocity (see Figures 24 and 25). To do so, we take advantage of two useful results:

1. As suggested by (90), for waves propagating perpendicular to the flow, the frequency is constant along a ray path assuming the coefficients (which describe the background flow) are not varying in time.

2. Assuming the wave field is in an energetic equilibrium, i.e. $\partial\langle E\rangle/\partial t = 0$, then $\langle E\rangle|\mathbf{c_g}|A$ is constant along a ray path, where A is a ray tube area (i.e. the distance of a line perpendicular to two nearby ray paths in two dimensions). Hence, we expect to see higher energy levels if waves are trapped and $\mathbf{c_g} \to 0$ or if rays converge.

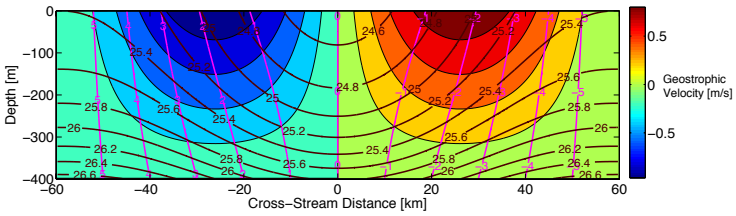

Figure 24: The streamwise velocity (color), potential density (black), and absolute momentum M_g (magenta).

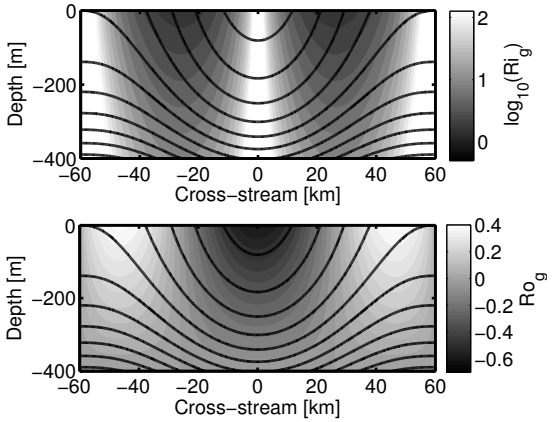

Figure 25: The base-10 logarithm of the Richardson number **(top)** and the Rossby number **(bottom)** for the idealized background flow (Figure 24). Potential density contours with an increment of .2 kg/m^3 are superimposed.

Rays for a trapped sub-inertial wave with $\omega = .95f$ are plotted in Figure 26 and compared with numerical solutions to the governing equation, which is essentially the Green's function for an oscillating point source.

See Whitt and Thomas (2013) *Near-inertial waves in strongly baroclinic currents* for further discussion.

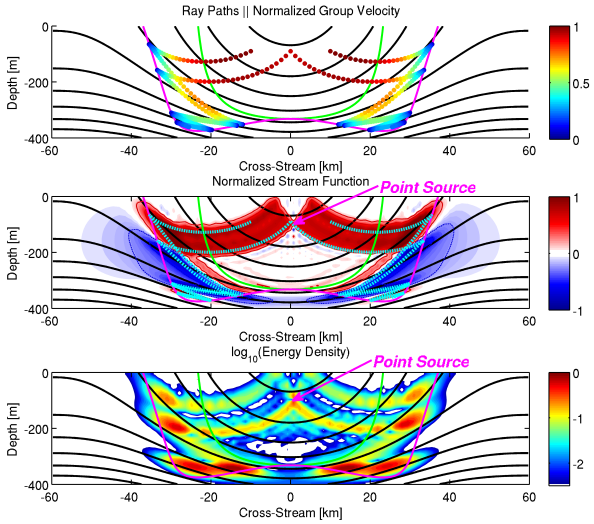

Figure 26: **Top:** Rays (parallel to characteristics) in the idealized background flow for waves with $\omega = .95f$. The variation of the magnitude of the group velocity (normalized by its maximum along each ray) is colored on the rays. **Middle:** A numerical solution to (124) with $\omega = .95f$ and a point source at $y \approx 0.75$ km, $z \approx -100$ m (this is essentially the Green's function for an oscillatory forcing at a point). This is a snapshot of the stream function in time and the dashed cyan lines are the same rays shown in the top panel. **Bottom:** Energy density, $\overline{E}$, associated with the numerical solution for Ψ shown in the middle panel. These figures confirm ray tracing is qualitatively similar to the numerical solution. High energy densities, velocities and shears occur near turning points and slantwise critical layers (defined in text) that run parallel to isopycnals.